HYDRAULIC FRACTURE OPTIMIZATION WITH A PSEUDO-3D MODEL IN MULTI-LAYERED LITHOLOGY

A Thesis

by

MEI YANG

Submitted to the Office of Graduate Studies of
Texas A&M University
in partial fulfillment of the requirements for the degree of

MASTER OF SCIENCE

August 2011

Major Subject: Petroleum Engineering

Hydraulic Fracture Optimization with a Pseudo-3D Model in Multi-layered Lithology

HYDRAULIC FRACTURE OPTIMIZATION WITH A PSEUDO-3D MODEL IN MULTI-LAYERED LITHOLOGY

A Thesis

by

MEI YANG

Submitted to the Office of Graduate Studies of
Texas A&M University
in partial fulfillment of the requirements for the degree of

MASTER OF SCIENCE

Approved by:

Chair of Committee,	Peter P. Valkó
Committee Members,	Christine Ehlig-Economides
	Raytcho Lazarov
Head of Department,	Stephen A. Holditch

August 2011

Major Subject: Petroleum Engineering

ABSTRACT

Hydraulic Fracture Optimization with a Pseudo-3D Model

in Multi-layered Lithology.

(August 2011)

Mei Yang, B. Sc., Guizhou University;

M. S., Texas A&M University

Chair of Advisory Committee: Dr. Peter P. Valko

Hydraulic Fracturing is a technique to accelerate production and enhance ultimate recovery of oil and gas while fracture geometry is an important aspect in hydraulic fracturing design and optimization. Systematic design procedures are available based on the so-called two-dimensional models (2D) focus on the optimization of fracture length and width, assuming one can estimate a value for fracture height, while so-called pseudo three dimensional (*p*-3D) models suitable for multi-layered reservoirs aim to maximize well production by optimizing fracture geometry, including fracture height, half-length and width at the end of the stimulation treatment.

The proposed *p*-3D approach to design integrates four parts: 1) containment layers discretization to allow for a range of plausible fracture heights, 2) the Unified Fracture Design (UFD) model to calculate the fracture half-length and width, 3) the PKN or KGD models to predict hydraulic fracture geometry and the associated net pressure and other treatment parameters, and, finally, 4) Linear Elastic Fracture Mechanics

(LEFM) to calculate fracture height. The aim is to find convergence of fracture height and net pressure.

Net pressure distribution plays an important role when the fracture is propagating in the reservoir. In multi-layered reservoirs, the net pressure of each layer varies as a result of different rock properties. This study considers the contributions of all layers to the stress intensity factor at the fracture tips to find the final equilibrium height defined by the condition where the fracture toughness equals the calculated stress intensity factor based on LEFM.

Other than maximizing production, another obvious application of this research is to prevent the fracture from propagating into unintended layers (i.e. gas cap and/or aquifer).

Therefore, this study can aid fracture design by pointing out:

(1) Treating pressure needed to optimize fracture geometry,

(2) The containment top and bottom layers of a multi-layered reservoir,

(3) The upwards and downwards growth of the fracture tip from the crack center.

DEDICATION

I would like to dedicate this work to my mother, Qunxian Zhao, for her encouragement and love.

ACKNOWLEDGEMENTS

I wish to express my gratitude to my committee chair, Dr. Peter Valko, for his help, advice and support throughout the entire course of this research.

My very special thanks and appreciation go to my committee members, Dr. Christine Ehlig-Economides for her valuable course, advice guidance and numerous helpful suggestions during my study and research. I wish to thank Dr. Raytcho Lazarov, for his guidance and support throughout the course of this research.

I thank Economides Consultant Inc.,Dr. Michael J. Economides, Mr. Matteo Marongiu-Porcu and Mr. Termpan Pitakbunkate for their valuable advice and suggestions for my research and for their friendship.

I appreciate my husband, Yi Huang, without whose support and understanding, this study would have been impossible. My adorable daughter, Keyang Huang, provided the necessary sweet moments whenever I encountered difficulties.

I also appreciate the help from the department faculty and staff. They offered their support, knowledge and work experience which were so helpful for my research.

Thanks also go to all of my friends at Texas A&M University for making my time a great and invaluable experience.

NOMENCLATURE

Symbol		Description
a	=	fracture half-height, L, ft
asp	=	fracture aspect ratio
A	=	reservoir drainage area, L^2, acre
A_f	=	fracture surface area, L^2, ft^2
b	=	layer's dimensionless location
$b_{perf,s}$	=	perforation start layer's dimensionless location
$b_{perf,e}$	=	perforation end layer's dimensionless location
c	=	proppant concentration, m/L^3, ppg
c_e	=	proppant concentration at the end of the job, m/L^3, ppg
c_{added}	=	added proppant concentration, m/L^3, ppga
C_{fD}	=	dimensionless fracture conductivity
C_L	=	leak-off coefficient, $L/t^{0.5}$, $ft/min^{0.5}$
d	=	true vertical depth
e	=	end
E	=	Young's modulus, m/Lt^2, psi
E'	=	plane strain modulus, m/Lt^2, psi
h_f	=	fracture height, L, ft
h_n	=	thickness of net pay, L, ft
h_p	=	thickness of perforation interval, L, ft

Δh_d	=	fracture growth into lower bounding formation, L, ft
Δh_u	=	fracture growth into upper bounding formation, L, ft
I_x	=	penetration ratio
J	=	well productivity index, L^4t^2/m, bbl/psi
J_D	=	well dimensionless productivity index
k	=	reservoir permeability, L^2, md
k_{00}	=	pressure at center of crack, m/Lt^2, psi
k_1	=	hydrostatic gradient, m/ L^2t^2, psi/ft
k_f	=	propped fracture permeability, L^2, md
K	=	rheology consistency index, m/Lt^2, lbf s^{npr}/ ft^2
K_I	=	stress intensity for opening crack, $m/L^{0.5}t^2$, psi-$in^{0.5}$
$K_{I,bottom}$	=	stress intensity at bottom tip of crack, $m/L^{0.5}t^2$, psi-$in^{0.5}$
$K_{I,top}$	=	stress intensity at top tip of crack, $m/L^{0.5}t^2$, psi-$in^{0.5}$
K_{IC}	=	fracture toughness, $m/L^{0.5}t^2$, psi-$in^{0.5}$
K_{IC2}	=	fracture toughness of upper layer, $m/L^{0.5}t^2$, psi-$in^{0.5}$
K_{IC3}	=	fracture toughness of lower layer, $m/L^{0.5}t^2$, psi-$in^{0.5}$
K'	=	modulus of cohesion, $m/L^{0.5}t^2$, psi-$in^{0.5}$
M_{prop}	=	proppant mass, m, lbm
$M_{prop,stage}$	=	proppant mass required for each stage, m, lbm
n	=	rheology flow behavior index
N_{prop}	=	proppant number

Δp	=	pressure difference, m/Lt^2, psi
p_b	=	breakdown pressure or rupture pressure, m/Lt^2, psi
p_c	=	fracture closure pressure, m/Lt^2, psi
$p_{c,p}$	=	pressure at center of perforation, m/Lt^2, psi
$p_{c,y}$	=	pressure at any location y, m/Lt^2, psi
p_r	=	fracture reopening pressure, m/Lt^2, psi
p_{net}	=	net pressure at center of perforation, m/Lt^2, psi
p_{nw}	=	net pressure at center of crack, m/Lt^2, psi
$p_n(x)$	=	net pressure at any location in x-direction, m/Lt^2, psi
$p_n(y)$	=	net pressure at any location in y-direction, m/Lt^2, psi
q_i	=	slurry injection rate for one-wing, L^3/t, bbl/min
q_p	=	production rate, L^3/t, bbl/min
r_e	=	reservoir drainage radius, L, ft
S_f	=	fracture stiffness, m/ L^{2}t^2, psi/in
S_p	=	spurt loss coefficient, L, ft
t_e	=	pumping time, t, min
t_{paD}	=	padding time, t, min
T_0	=	tensile strength, m/Lt^2, psi
u_{avg}	=	average velocity of slurry in fracture, L/t, ft/s
V_f	=	fracture volume, L^3, ft^3

V_i	=	total slurry injection volume, L^3, ft^3
V_{paD}	=	padding volume, L^3, gal
V_{prop}	=	proppant volume, L^3, ft^3
V_{res}	=	reservoir volume, L^3, ft^3
V_{stage}	=	liquid volume required for each stage, L^3, gal
w	=	propped fracture width, L, in
$\overline{w}$	=	average hydraulic fracture width, L, in
$w_0(x)$	=	max. hydraulic fracture width at any location, L, in
$w_{w,0}$	=	max. hydraulic fracture width at wellbore, L, in
x_e	=	reservoir length, L, ft
x_f	=	fracture half-length, L, ft
y	=	dimensionless vertical position
y_d	=	dimensionless vertical position of bottom perforation
y_u	=	dimensionless vertical position of top perforation

Greek

γ	=	shape factor
γ_w	=	surface energy of fracture, mL/t^2, $psi\text{-}ft^2$
ε	=	exponent of the proppant concentration curve
$\in$	=	strain
κ	=	Nolte's function at $\Delta t = 0$
η	=	slurry efficiency

η_0 = ratio of fracture volume in net pay to total fracture volume

ϕ_p = fracture packed porosity

ρ_p = proppant density, m/ L^3, lbm/ft^3

σ = normal stress, m/Lt^2, psi

$\sigma(y)$ = normal stress at any location in y-direction, m/Lt^2, psi

σ_h = minimum horizontal in-situ stress, m/Lt^2, psi

σ_H = maximum horizontal in-situ stress, m/Lt^2, psi

$\Delta\sigma_{avg}$ = average stress difference, m/Lt^2, psi

$\Delta\sigma_d$ = stress diff. of reservoir and lower formation, m/Lt^2, psi

$\Delta\sigma_u$ = stress diff. of reservoir and upper formation, m/Lt^2, psi

τ = shear stress, m/Lt^2, psi

μ = viscosity, m/Lt, cp

μ_e = equivalent Newtonian viscosity, m/Lt, cp

μ_f = friction coefficient, L, in

ν = Poisson's ratio

TABLE OF CONTENTS

Page

Page

LIST OF FIGURES

Page

Page

LIST OF TABLES

Page

1. INTRODUCTION

Hydraulic fracturing is a technique to stimulate the production of oil and gas wells. In this exercise, the fracture geometry optimization is an important aspect. The most commonly used two-dimensional models (2D) focus on the optimization of fracture length and width, assuming the fracture height is constant. This approach was the central theme of the UFD. Pseudo three dimensional (*p*-3D) models consider fracture height migration and thus a more appropriate description of fracture geometry that now includes the fracture height in addition to the half-length and width. *p*-3D models are used routinely for predicting fracture geometry in multi-layered reservoirs, but are more difficult to use in an optimization mode.

Pitakbunkate (2010) presented a *p*-3D design procedure in a three-layer reservoir with contrasting lithology. The result is satisfactory but some observations are warranted which have led to this work. In applying the equilibrium height concept to a three-layer system there are upper and lower limits in the net pressure, which if not adhered to, would lead to an unstable solution and an unsuccessful design. The proposed *p*-3D multilayer model is not burdened by such constraints: there is no artificial restriction on rock properties and fracture propagation.

Another advantage of this research is that the model is designed under multi-zone lithology which is closer to the real reservoir situation than a three-layer model.

The proposed *p*-3D model integrates four parts

_____

This thesis follows the style of *SPE Journal.*

- containment layers discretization to allow for a range of plausible fracture heights,
- the Unified Fracture Design (UFD) model to calculate the fracture half-length and width,
- the PKN or KGD models to predict hydraulic fracture geometry and the associated net pressure and other treatment parameters, and, finally,
- Linear Elastic Fracture Mechanics (LEFM) to calculate fracture height

UFD sizes the fracture geometry to provide a physical optimization to well performance. The Proppant Number is used as a correlating parameter, which in turn provides the maximum dimensionless productivity index ($J_{D,max}$), corresponding to the optimum dimensionless fracture conductivity, $C_{fD,opt}$. Once the latter is determined, the fracture dimensions, i.e., fracture length and width, are set.

However, UFD assumes the knowledge of the proppant volume reaching the pay zones. Fracture height growth can substantially affect the distribution of proppant, and hence the Proppant Number itself. The net pressure distribution plays an important role when the fracture is propagating in the reservoir. In a multi-layered reservoir, the net pressure of each layer varies as a result of different rock properties. This study involves the contributions of all layers to the stress intensity factors at the fracture tips and finds the final equilibrium height from the condition that the fracture toughness equals the stress intensity factor calculated from LEFM. In other words, the Griffith criterion states that a fracture will advance when the stress intensity at the tip reaches a critical value, K_{IC}. This critical value is a rock property and can be determined experimentally.

Other than maximizing production, another obvious application of this research is to prevent the fracture from propagating into the unintended layers (i.e. gas cap and aquifer).

Therefore, this study can guide fracture design by pointing out: treating pressure needed to optimize fracture geometry as well as containment layers of the multiple layers the fracture propagation will stop at, given the above treating pressure.

Fracture geometry optimization is a key to a hydraulic fracturing design. Researches on the fracture geometry include:

Two-dimensional (2D) models, as:

Perkins and Kern (1961), PKN model, Figure 1 (a); Khristianovitch, Geertsma and De-Klerk(1955), KGD model, Figure 1 (b); and Radial Model;

Three-dimensional (3D) and pseudo-3 dimensional (p3D) models, as:

"Cell" approach, Figure 1 (c),(Cleary 1994) ; overall fracture geometry parameterization, Figure 1 (d); and meshed full 3D model, Figure 1 (e),(Johnson et al., 1993.)

1.1. Background and Literature Review

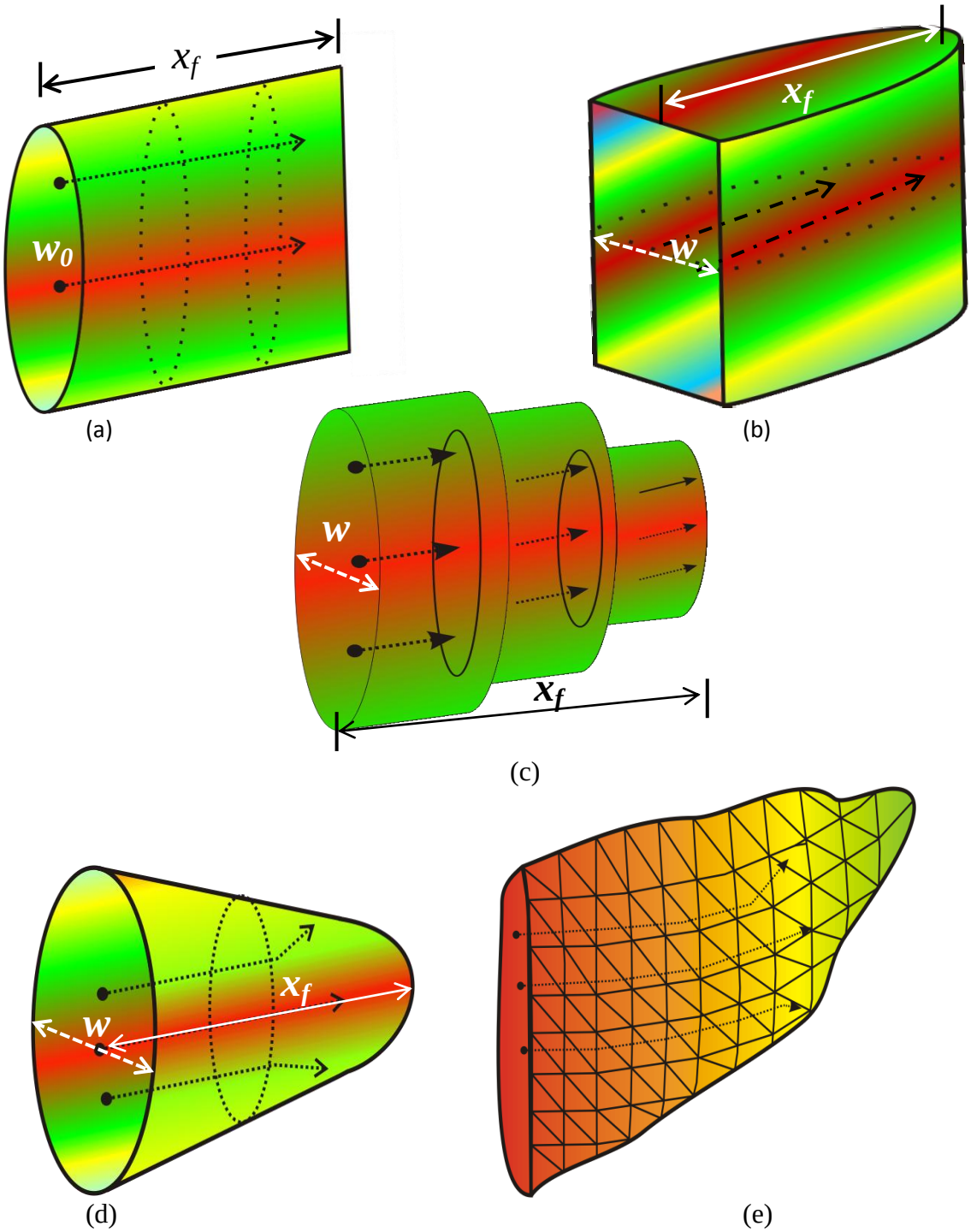

Figure 1 : Fracture geometry (a) PKN type (b) KGD type (c) Pseudo 3D cell approach (d) Global 3D, parametrised (e) Full 3D, meshed

Fracture geometry optimization is a key to a hydraulic fracturing design. Researches on the fracture geometry include:

Two-dimensional (2D) models, as:

Perkins and Kern (1961), PKN model, Figure 1 (a); Khristianovitch, Geertsma and De-Klerk(1955), KGD model, Figure 1 (b); and Radial Model;

Three-dimensional (3D) and pseudo-3 dimensional (p3D) models, as:

"Cell" approach, Figure 1 (c),(Cleary 1994) ; overall fracture geometry parameterization, Figure 1 (d); and meshed full 3D model, Figure 1 (e),(Johnson et al., 1993.)

While a 2D model is focusing on the fracture length and width by assuming one can estimate a value for fracture height, the 3D and p-3D models attempt to predict height along with length and width.

Fracture crack behavior was analyzed by Griffith (1921) under tensile-loading conditions, by assuming microcracks of elliptic shape with a small minor axis. That vision was modified and restated in Linear Elastic Fracture Mechanics (LEFM) by Orowan (1952) and Irwin (1957). Rice (1968) derived an expression to calculate stress intensity factor.

Eekelen (1982) considered the factors impacting fracture containment. A number of factors (in-situ stress contrast, elastic properties, fracture toughness, ductility, and permeability) were studied and the conclusion was that stiffness contrast and in-situ stresses between zones were the most crucial variables.

Economides, Oligney and Valko (2002) developed the Unified Fracture Design (UFD), which provides a mechanism to determine the optimal hydraulic fracture design for a given amount of a selected proppant, while modern hydraulic fracture treatment execution offers the potential to achieve the optimal design. The Proppant Number links the crack behavior with production optimization.

The optimized fracture half-length, by PKN or KGD model, can determine the hydraulic fracture width. Perkins and Kern (1961) assumed that a fixed height vertical fracture propagates in a well-confined zone. The PKN model assumes that the condition of plane strain holds in every vertical plane normal to the direction of propagation which means that each vertical cross section deforms individually and is not affected by neighbors. In addition to the plane strain assumption, the fracture fluid pressure is assumed to be constant in the vertical cross section which is perpendicular to the direction of propagation. The fracture cross section is elliptical with the maximum width at the center proportional to the net pressure at the point. Kristianovich and Zheltov (1955) derived a solution for the propagation of a hydraulic fracture with a horizontal plane strain assumption. As a result, the fracture width does not depend on the fracture height, except through the boundary condition at the wellbore. The fracture has rectangular cross section and its width is constant in the vertical plane. The fluid pressure gradient in the propagating direction is determined by the flow resistance in a narrow rectangular slit of variable width in the vertical direction.

Geetsma and Hafkens (1979) believed the PKN model is more appropriate for long fractures ($\frac{2x_f}{h_f} \geq 1$) while KGD model is applicable for short fractures, ($\frac{2x_f}{h_f} \leq 1$) .

Pitakbunkate (2010) did research on *p*-3D model in a three-layer lithology reservoir, predicting fracture height, half-length and width at the end of fracture job.

1.2. Objectives of Research

This research has primarily concentrated on incorporating a p-3D hydraulic fracturing propagation model into the systematic design of a fracturing treatment for for oil and gas multi-layered reservoirs.

There are a number of considerations in optimizing fracture dimensions to maximize the production. The reservoir deliverability, well producing systems, fracture mechanics, fracturing fluid characteristics, proppant transport mechanism, operational constraints and economics should be considered and integrated in order to achieve the optimized design, therefore maximize the benefit of a stimulation treatment.

Pitakbunkate (2010) did research on *p*-3D model in a three-layer lithology reservoir. One drawback of this model is some constrains are needed to ensure a solution.

For example, Figure 2 illustrates that the final solution lies out of the valid range of original equilibrium height. In such cases, artificial constraints are applied to ensure the solution. One of them is to assume the fracture migrates the same depth upwards and downwards. Another assumption is that the net pressure at the end of the job equals the average stress difference of the reservoir and adjacent layers ($\boldsymbol{p_{net}} = \Delta\boldsymbol{\sigma}$).

The proposed approach in this research is a forward calculation method, by accounting for all the possible solutions within a certain threshold of accuracy and check if the

bonding equations are satisfied simultaneously. It will not rely on any constraints and there is no need for artificial restrictions on rock properties and fracture propagation. Another advantage of this work is that the model is designed under multi-zone lithology which is closer to the real reservoir situation than a three-layer model. This package can be used to point out upward and downward containment layers.

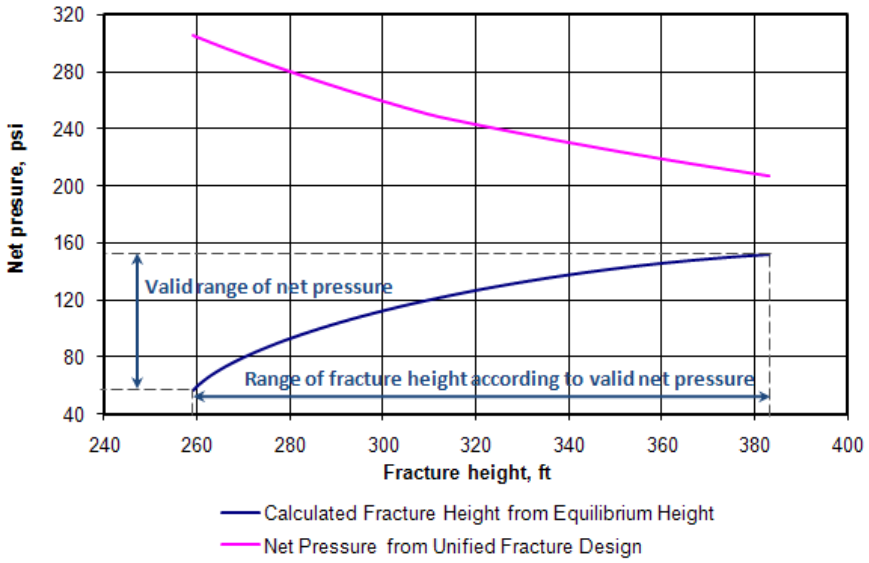

Figure 2 : ***p*-3D equilibrium height calculation, solution has a limit in the valid range of calculation (Pitakbunkate T. 2010)**

2. BASIC CONCEPT

2.1. Introduction to Hydraulic Fracturing Design Technology

Hydraulic fracturing (propped fracturing) is one of the completion techniques to improve well performance. From the very first intentional hydraulic fracturing job, in the Hugoton gas field in western Kansas, 1947, tens of thousands of fracture jobs are completed every year, ranging from small “skin-bypass” fracs to massive treatments. Many fields produce only because of hydraulic fracturing technology. For example all unconventional gas wells need horizontal well completions with multiple transverse fractures (Economides and Martin, 2007).

Fracturing will stimulate the production not only of a low permeability formation, but also for those wells which have large skin factor because of drilling fluid damage, for higher-permeability, soft-formation, wells which need sand control.

For a hydraulically fractured well the manner with which fluids flow in the well is altered significantly from what would have been under radial flow. The hydraulic fracture allows for the fluids to flow linearly from the reservoir into the fracture and then linearly along the fracture into the well. A common name for this is bi-linear flow. The fracture provides for a low-pressure drawdown compared to radial flow and therefore, productivity index increases. From another point of view, after fracturing, the dominating flow regime changes from radial to linear flow, as shown in Figure **3** .

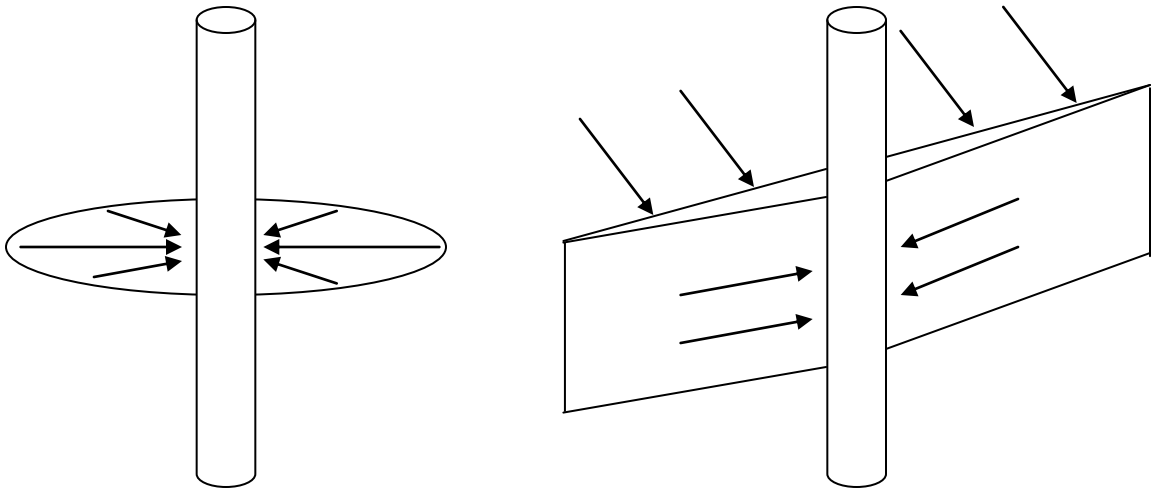

Figure 3 : **Flow regime changes before (left) and after (right) hydraulic fracturing**

The proposed *p*-3D model of the multi-layered reservoir integrates four parts, including containment layers discretization to get the possible fracture height candidates, Unified Fracture Design (UFD) model to calculate the fracture half-length and width, PKN/KGD model to calculate net pressure, and Linear Elastic Fracture Mechanics (LEFM) to calculate equilibrium fracture height.

In this research, the add-in fracture design program (Section 2.6) for treatment schedule determination is based on the fixed proppant mass and fracture height. With the given proppant mass and fracture height, fracture half-length can be determined using UFD methodology. After the fracture length is obtained, the simple fracture propagation models (2D fracture-propagation models) are used to predict the hydraulic fracture width at the end of pumping.

2.2. Rock Mechanical Characteristics

If a force, *F*, is applied on a body with cross sectional area, *A*, perpendicular to the direction of action of the force, then the stress, $\boldsymbol{\sigma}$ induced in this body is defined as:

$$\sigma=\frac{F}{A} \tag{1}$$

In-situ stresses are the stresses within the formation, acting as a load on the formation. They come mainly from the overburden, the sum of all the pressures induced by all the different rock layers; tectonics, volcanism and plastic flow etc. The former is given by Eq. (**2**) while the latter is hard to predict. For simplicity purpose, we ignore those factors in this research, although they can significantly affect the in-situ stresses.

$$\boldsymbol{\sigma_v} = \sum_{0}^{n} \boldsymbol{\rho_i g h_i} \tag{2}$$

where ρ_i is the density of layer *i*, *g* is the acceleration due to gravity and h_i is the thickness of zone *i*, for a subsurface formation with n zones.

Fractures will always propagate along the path of least resistance. In a 3D stress regime, a fracture will propagate parallel to the greatest principle stress ($\sigma_{h,\max}$) and perpendicular to the minimum principal stress ($\sigma_{h,\min}$), as Figure 4. The horizontal stress in an undisturbed formation is defined as

$$\sigma_h = (\sigma_v - \alpha p_r)\frac{v}{1-v} + \alpha p_r \tag{3}$$

where $\boldsymbol{\sigma_v}$ is the overburden pressure and $\boldsymbol{p_r}$ is the pore pressure, $\boldsymbol{\alpha}$ is Biot's poroelastic constant, *v* is the Poisson ratio.

For the 2D fracture model, the PKN and KGD are two models commonly accepted. PKN model is more appropriate for long fractures while the KGD model is applicable for short fractures.

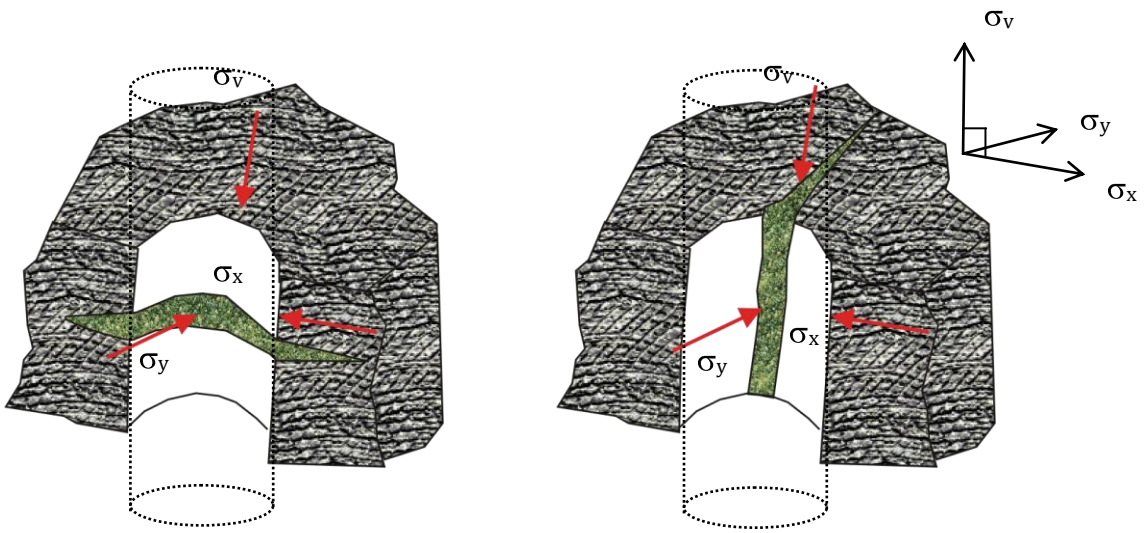

(a) Horizontal fracture (b) Vertical fracture

Figure 4 : Fracture propagation perpendicular to the least principle stress

2.1.1. PKN-type Fracture Geometry

Perkins and Kern (1961) assumed that a constant height vertical fracture is propagated in well-confined zone. The PKN model assumes that the condition of plane strain holds in every vertical plane normal to the direction propagation. Also there is no slippage between the formation boundaries; the width is proportional to fracture height. The fracture cross section is elliptical with the maximum width at the center proportional to the net pressure at the point, as Figure 1(a).

The maximum width can be calculated using Eq.(4).

$$w_0 = \frac{2h_f\, p_n(x)}{E'} \tag{4}$$

where E' is the plane strain modulus which is given by Eq. (5)

$$E' = \frac{E}{1-\nu^2} \tag{5}$$

Since the net pressure at the tip of the fracture is zero, and the fluid pressure gradient in the propagating direction is determined by the flow resistance in a narrow, elliptical flow channel:

$$\frac{\partial p_n(x)}{\partial x} = -\frac{4\mu q_i}{\pi w_0^{\,3} h_f} \tag{6}$$

Combining Eq. (4) and (6), integrating with the zero net pressure condition at the tip, the maximum fracture width profile at any location in the direction of propagation can be derived as shown in Eq.(7).

$$w_0(x) = w_{w,0}\left(1-\frac{x}{x_f}\right)^{1/4} \tag{7}$$

where $w_{w,0}$ is the maximum hydraulic fracture width at the wellbore which is given in consist system of units by

$$w_{w,0} = 3.27\left(\frac{\mu q_i x_f}{E'}\right)^{1/4} \tag{8}$$

The above equation is used to calculate the maximum width at the wellbore. In order to finding the average width of the fracture, the maximum width must be multiplied by the shape factor, γ, which contains two elements. The first one which is $\pi/4$ is the factor to average the ellipse width in the vertical plane and the other one is the laterally averaged factor which is equal to $4/5$.

$$\overline{w} = \gamma w_{w,0} = \frac{\pi}{4}\frac{4}{5}w_{w,0} = \frac{\pi}{5}w_{w,0} \tag{9}$$

Assuming that q_i, x_f and E' are known, the only unknown in Eq. (8) for maximum fracture width calculation is μ. Using the formula for equivalent Newtonian viscosity of Power law fluid flowing in a limiting ellipsoid cross section:

$$\mu_e = K\left[\frac{1+\left(\frac{1}{n}-1\right)n}{\pi n}\right]^n\left(\frac{2\pi u_{avg}}{w_0}\right)^{n-1} \tag{10}$$

where u_{avg} is linear velocity:

$$u_{avg} = \frac{q_i}{h_f \overline{w}} \tag{11}$$

and combining the Eq. (8) to Eq.(11), the maximum fracture width at the wellbore can be solved as shown below.

$$w_{w,0} = 3.98^{\frac{n}{2+2n}} 9.15^{\frac{1}{2+2n}} K^{\frac{1}{2+2n}}\left(\frac{1-\left(\frac{1}{n}-1\right)n}{n}\right)^{\frac{n}{2+2n}}\left(\frac{h_f^{1-n} q_i^n x_f}{E'}\right)^{\frac{1}{2+2n}} \tag{12}$$

2.1.2. KGD-type Fracture Geometry

Kristianovich and Zheltov (1955) derived a solution for the propagation of a hydraulic fracture in which the horizontal plane strain is held. As a result, the fracture width does not depend on the fracture height, except through the boundary condition at the wellbore. The fracture has rectangular cross section, as Figure 1(b), and its width is constant in the vertical plane because the theory is based on the plane strain condition, which was applied to derive a mechanically satisfying model in individual horizontal planes. The fluid pressure gradient in the propagating direction is determined by the flow resistance in a narrow rectangular slit of variable width along the horizontal direction.

The maximum fracture width profile is same as the PKN model, Eq. (**4**) through Eq. (**7**), and the KGD width equation is

$$w_{w,0} = 3.22\left(\frac{\mu q_i x_f^{\,2}}{E' h_f}\right)^{1/4} \tag{13}$$

The average fracture width of this model is (has no vertical component)

$$\overline{w} = \gamma w_{w,0} = \frac{\pi}{4} w_{w,0} \tag{14}$$

The final equation to determine the maximum fracture width of the KGD model is

$$w_{w,0} = 3.24^{\frac{n}{2+2n}} 11.1^{\frac{1}{2+2n}} K^{\frac{1}{2+2n}} \left(\frac{1+2n}{n}\right)^{\frac{n}{2+2n}} \left(\frac{q_i^n x_f^{\,2}}{E' h_f^n}\right)^{\frac{1}{2+2n}} \tag{15}$$

2.3. Mini-Frac

From the rock mechanics side, a crack will be initiated only if the introduced pressure overcomes the breakdown pressure of the rock formation. Hubbert and Willis (1957) showed that whenever the stress field is anisotropic, fracture propagates in the plane perpendicular to minimum principal in-situ stress (Figure 5) because the fracture prefers to take the path of least resistance and therefore opens up against the smallest stress. Once the fracture is created, as long as the pressure is greater than the stress normal to the plane of the fracture which is equal to the closure pressure, p_c, it will continue to propagate.

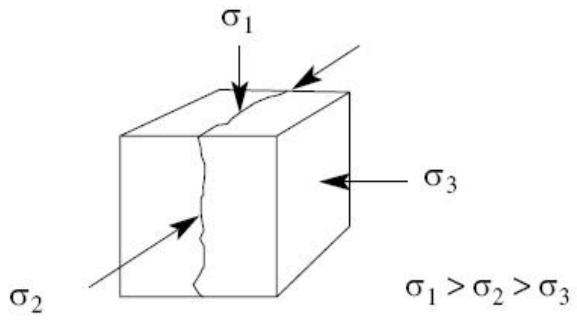

Figure 5 : **Effect of in-situ stresses on fracture azimuth**

Mini-frac analysis is designed to determine initial stresses; minimum in-situ stress, σ_h, maximum in-situ stress, σ_H, and the leak-off coefficient.

The fracture fluid is injected into the well and pressurized to create a fracture in the reservoir. To initiate the crack in the reservoir, the downhole pressure must overcome the breakdown pressure (the peak of the first cycle). After the crack is created, the downhole pressure decreases while fracture continues to propagate into the reservoir. The fracture closure pressure can be evaluated after injection is stopped. The observation of the closure pressure is shown in Figure 6. The second cycle almost seems identical to the first one. However, it requires lower downhole pressure to reopen the fracture (reopening pressure, p_r) in the reservoir than it does for fracture creation ($p_b > p_r$).

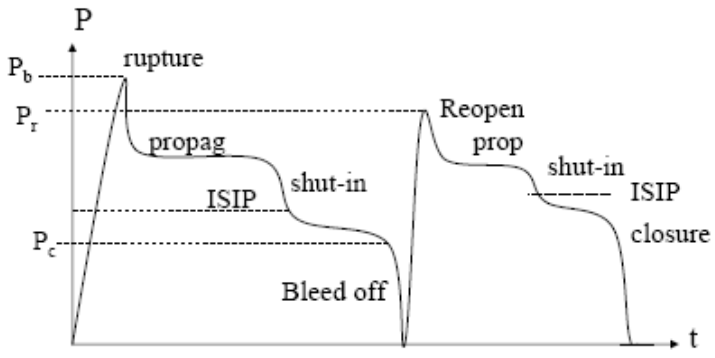

Figure 6 : **Pressure profile of fracture propagation behavior**

2.4. Unified Fracture Design

Economides et al. (2002) introduced the concept called Unified Fracture Design (UFD). It offers a method to determine the fracture dimensions providing the maximum reservoir performance after fracturing with the given amount of proppant. From an economic point of view, optimization requires the balancing of benefits vs costs. However in all cases the maximum reservoir performance, i.e., maximizing the production rate is essential. The

parameter, which represents the production rate very well, is the productivity index. As a result, in the UFD, the dimensionless productivity, J_D, is observed.

$$J_D = \frac{141.2 q_p B \mu}{k h \Delta p} \tag{16}$$

The Proppant Number, N_{prop}, is an important parameter for the UFD. The proppant number is a dimensionless parameter and is defined as

$$\mathrm{N}_{\mathrm{prop}} = I_x^2 C_{fD} \tag{17}$$

where I_x is the penetration ratio and C_{fD} is the dimensionless fracture conductivity.

The penetration ratio is the ratio of the fracture length, $2x_f$, to the equivalent reservoir length, x_{e} . The dimensionless fracture conductivity is the ratio of the flow potential from the fracture to the well to that from the reservoir to the fracture as shown in Eq. (19). The correlation of the equivalent reservoir length and the reservoir radius is shown in the Eq.(20) **.**

$$I_x = \frac{2x_f}{x_e} \tag{18}$$

$$C_{fd} = \frac{k_f w}{k x_f} \tag{19}$$

$$A = r_e{}^2 \pi = x_e{}^2 \tag{20}$$

Substituting Eq. (18) and (19) into Eq. (17), the correlation to determine the proppant number can be written as

$$\mathrm{N}_{\mathrm{prop}} = \frac{4 k_f x_f w}{k x_e{}^2} = \frac{2k_f}{k} \frac{2x_f w h_n}{x_e{}^2 h_n} = \frac{2k_f}{k} \frac{V_{prop}}{V_{res}} \tag{21}$$

where V_{prop} is the volume of the propped fracture in the net pay. This number can be determined from the mass of proppants for the fracturing operation. However, the

proppants do not only go in net pay but also fill the whole fracture. In order to use the mass of proppants to estimate V_{prop}, it requires multiplying with the ratio of the net height to the fracture height.

$$V_{prop} = \frac{M_{prop}\eta_0}{(1-\phi_p)\rho_p} \approx \frac{M_{prop}\left(\frac{h_n}{h_f}\right)}{(1-\phi_p)\rho_p} \tag{22}$$

From the calculated proppant number, the maximum dimensionless productivity index can be computed using the correlation as shown in Figure 7 and Figure 8. From the plot, the dimensionless fracture conductivity corresponding to the maximum productivity index can be determined. Then, the penetration ratio, the fracture half-length and the propped fracture width can be calculated using Eq. (17), (18) and (19). After obtaining the fracture dimensions, the treatment schedules must be determined based on this fracture geometry in order to achieve the maximum productivity index.

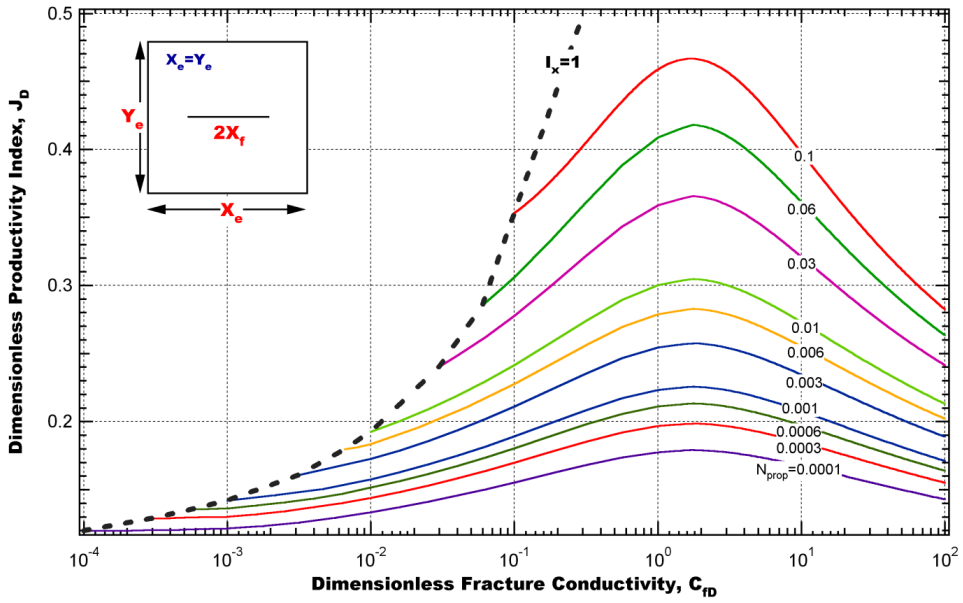

Figure 7 : **Dimensionless productivity index as a function of dimensionless fracture conductivity for** $N_{prop} < 0.1$ **(Economides et al., 2002)**

It is important to note that the Proppant Number includes only that part of the injected proppant volume that reaches the pay layers. In other words, the UFD approach can be used only if some assumptions have been made regarding the created fracture height and the resulting proppant placement.

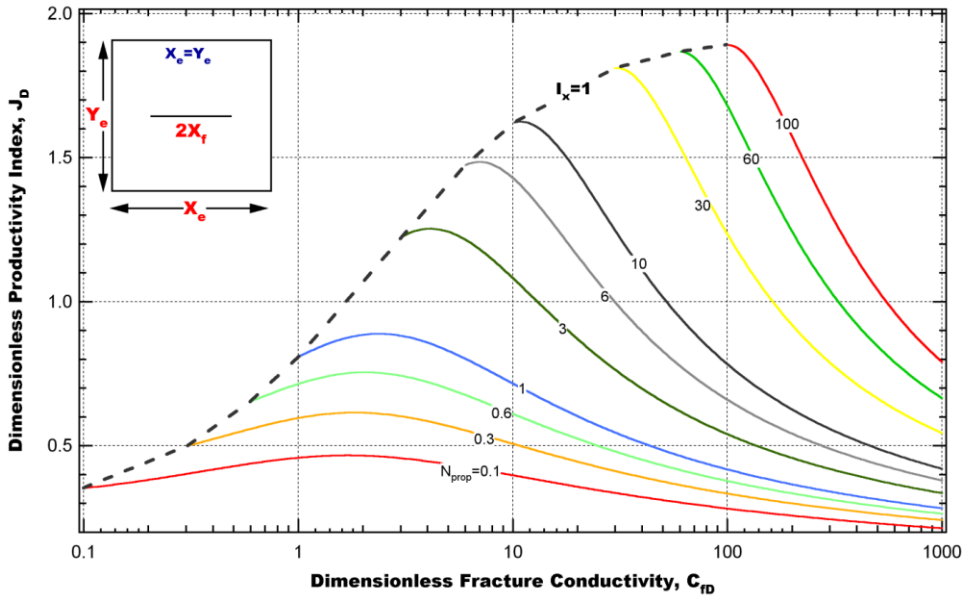

Figure 8 : **Dimensionless productivity index as a function of dimensionless fracture conductivity for** $N_{prop} > 0.1$ **(Economides et al., 2002)**

Once the optimum dimensionless fracture conductivity is known, the optimum fracture dimensions, i.e., propped fracture half length ($x_{f,opt}$) and propped fracture width ($w_{p,opt}$), are set:

$$x_{f,opt} = \frac{k_f V_f}{C_{fD,opt} k h_n} \tag{23}$$

$$w_{p,opt} = \frac{C_{fD,opt} k V_f}{k_f h_n} \tag{24}$$

As permeability rises, it becomes increasingly difficult to produce sufficient width without also generating excessive length. This permeability range is in the region of 25 to 50 md. Above this range, it is necessary to use a technique known as the Tip Screenout (TSO) to artificially generate extra width.

For hard rock, k<< 1 md, Eq. (23) and (24) are used to estimate the fracture geometry while for soft formation, k>> 1 md, Eq. (25)and (26) are appropriate to estimate the values, where they replace the optimum fracture conductivity in Eq. (23) and (24) with 1.6 .

$$x_{f,opt} = \frac{\overline{k_f V_f}}{1.6\, k h_n} \tag{25}$$

$$w_{p,opt} = \frac{\overline{1.6\, k V_f}}{k_f h_n} \tag{26}$$

2.5. Equilibrium Height Calculation

Fracture will stop if the stress (energy) reaches equilibrium, in other words, fracture toughness at the tip equals the stress intensity factor as per Eq. (27) and Eq.(28).

Eekelen (1982) concluded that in most cases the fracture would penetrate into the layers adjoining the perforation zone. A number of factors: in-situ stress contrast, $\Delta\sigma$, elastic properties, fracture toughness or stress intensity factor, K_I, ductility, D, permeability, k, and the bonding at the interface impact whether an adjacent formation will act as a fracture barrier. In this study, the depth of penetration is determined by the differences in stiffness and in horizontal in-situ stress contrast.

Linear Elastic Fracture Mechanics (LEFM) predicts how much stress is required to propagate a fracture. It assumes that linear elastic deformation (constant Young's

modulus) followed by brittle fracture, which means there is no energy lost due to plastic deformation or other effects and that all energy in the material is transferred to fracture propagation.

Griffith (1921) is the first who analyzed the cracks behavior in glass under tensile-loading conditions, under the assumption that the microcracks were elliptical with a small minor axis and used an energy ascribed to the newly released crack surface energy.

Orowan (1952) modified LEFM and Irwin (1957) restated it to include dissipative energy processes. LEFM states that a fracture will advance when its stress intensity reaches a critical value, K_{IC}, assuming that the crack tip is in a state of plane strain. K_{IC} is known as the plane-strain fracture toughness and has been shown to be a measurable material property.

Irwin (1957) classified three different singular stress fields according to the displacement. Mode I is opening, Mode II is in-plane sliding (shearing), and Mode III is anti-plane sliding of crack (tearing). For hydraulic fracturing problem, only the opening mode is involved and stress intensity respecting to Mode I is denoted by K_I.

Rice (1968) derived an expression to calculate Mode I stress intensity factor for a crack extending from $-a$ to $+a$ on the y axis as shown in the figure on page 29.

$$K_I = \frac{1}{\sqrt{\pi a}} \int_{-a}^{a} p(y_m) \sqrt{\frac{a + y_m}{a - y_m}} dy_m \qquad (27)$$

The fracture height calculation procedure was proposed by Simonson et al. (1976) for a symmetric geometry, but can be generalized to more complex situations. Basically, the method aims at the calculation of the equilibrium height of the hydraulic fracture for a

given internal pressure in a layered-stress environment. The equilibrium height satisfies the condition that the computed stress intensity factors at the vertical tips (top and bottom) are equal to fracture toughness of the layer as illustrated at the right part of the figure shown on page 29.

$$K_I = K_{IC} \tag{28}$$

Equation (28) should be satisfied at the two fracture tips. Because we do not know ahead in which layers the fracture tips are, not only the left-hand side (the calculated stress intensity factor) but also the right hand side (the fracture toughness) might be unknown at the start of the design procedure.

2.6. Fracturing High Rate Gas Well

The optimized fracture geometry design for high rate gas well differs from the oil well due to the likely non-Darcy effects in the gas reservoir. As discussed in Section 2.2), the Proppant Number is a key parameter. In the high rate gas well with non-Darcy flow in the fracture, the fracture permeability in Eq. (21) should be replaced by "effective permeability or non-Darcy permeability, which accounts for the additional pressure in the porous medium, in this case, the propped fracture.

Lopez et al. (2004) summarized different correlation to calculate Reynolds Number, then Proppant Number, as Figure 9 and Figure 10, this research used Ergun's correlation, Eq.(29).

$$\mathrm{k}_{\mathrm{N.D.}} = \frac{k_{lam}}{\frac{7}{600} N_{\mathrm{Re},PM.} + 1} = \frac{k_{lam}}{\frac{7\sqrt{6}}{120} \frac{1}{\varepsilon^{3/2}} \frac{\sqrt{k_{lam}} V_s \rho}{\mu} + 1} \tag{29}$$

where $N_{Re,PM}$ is the porous medium Reynolds number, defined in Eq.(30) ε is the porosity, μ is the fluid viscosity, k_{lam} is the laminar permeability. V_s is the superficial velocity and ρ is the fluid density.

$$N_{\mathrm{Re},PM.} = \frac{D_p V_s \rho}{\mu(1-\varepsilon)} = \sqrt{150}\sqrt{\mathrm{k}_{\mathrm{lam}}}\frac{1}{\varepsilon^{3/2}}\frac{V_s \rho}{\mu} \qquad (30)$$

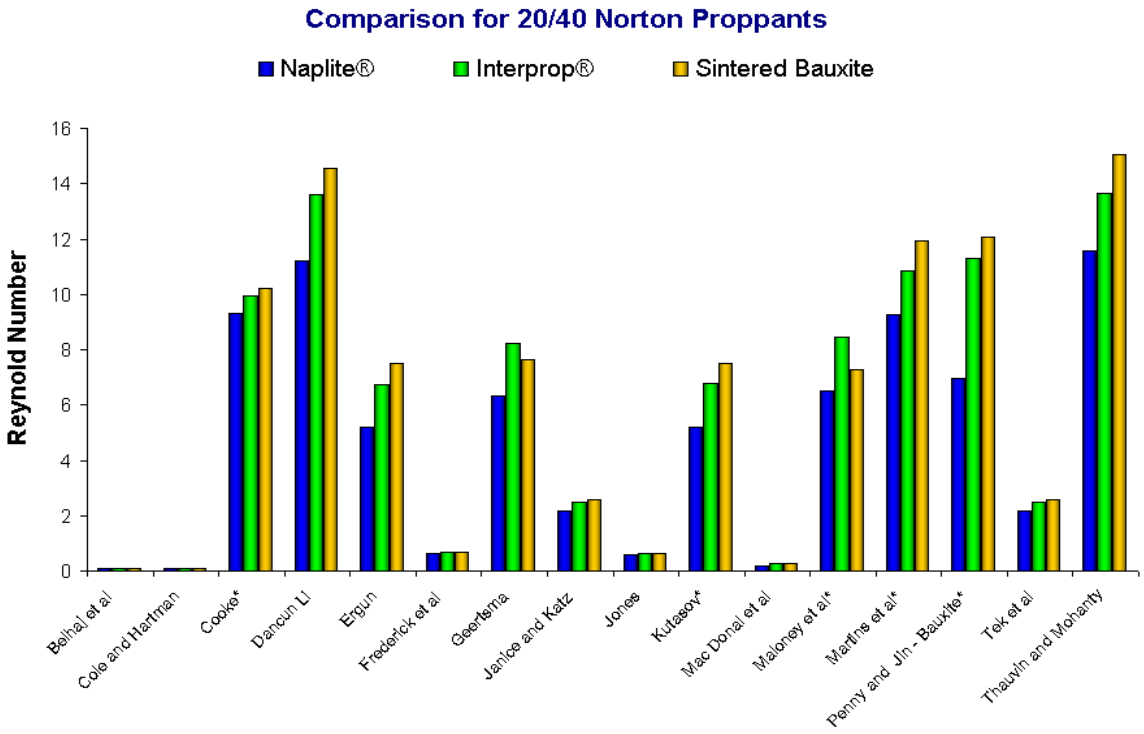

Figure 9 : Reynolds Number calculated from different correlation (Lopez et al., 2004)

Economides et al. (2002a) developed an iterative procedure to calculate the effective permeability. The flow chart is in Figure 11.

This study involves the Non-Darcy effect when considering gas well production as Section 3, example 2 illustrates.

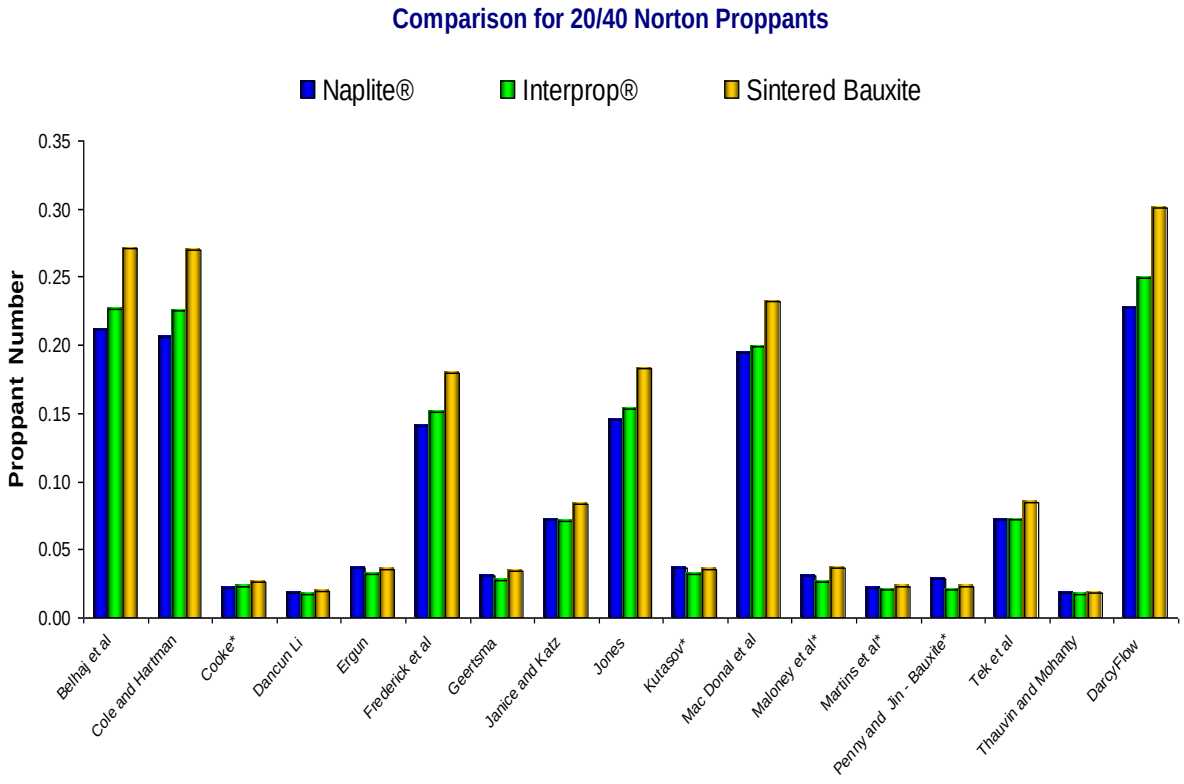

Figure 10:Proppant Number calculated from different correlation (Lopez et al., 2004)

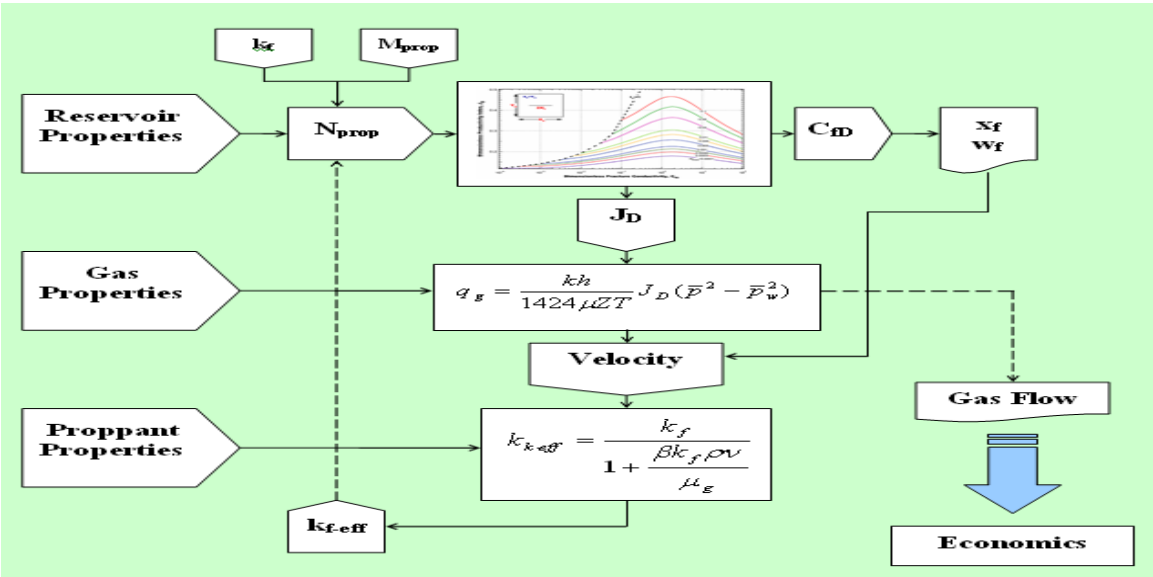

Figure 11:Effective permeability calculation flow chart

2.7. Pumping Schedule

To deliver the ideal fracture geometry discussed above, other than considering the rock properties, other important issues are fracturing fluid characteristics and the proppant transport mechanism.

The main function of the fracturing fluid is to create and extend the fracture, to transport proppant through the mixing and pumping equipment and into the fracture, and to place the proppant at the desired location in the fracture. Failure to adequately perform any one of these functions may compromise the stimulation job.

Valko listed fracturing fluid properties requirement in Modern Fracturing, 2007, Chapter 7:

1. Sufficient viscosity to create a fracture and transport the proppant,
2. Compatibility of the fluid with the formation to minimize formation damage,
3. A reduction in fluid viscosity after the proppant is placed to maximize fracture conductivity.

In proppant transport, various mechanisms can be responsible for the transportation, depending on the settling velocity of the proppant. The transition between the negligible and significant settling velocity mainly depends on two factors: the apparent viscosity of the fluid and the density difference between the proppant material and fluid, Aboud and Melo (Modern Fracturing, 2007).

The pumping schedule couples elasticity, flow and material balance. Figure 12 illustrates the proppant concentration distribution at the end of pumping.

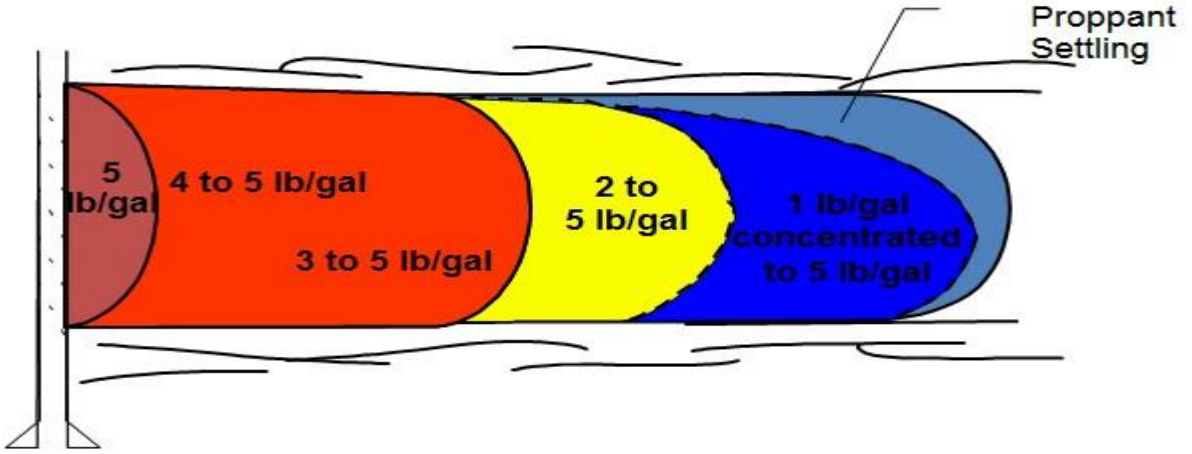

Figure 12: Stages at end of pumping

A typical fracture design procedure consists of two main parts.

First stage of the design includes:

1. The injection time calculation

$$\left(\frac{q_i}{h_f x_f}\right) t - 2\kappa C_L \sqrt{t} - (\overline{w}_e + 2S_p) = 0 \tag{31}$$

where h_f, x_f are desired fracture height and half-length. $\overline{w}_e$ is the average width in PKN model,

$$\overline{w}_e = 0.628 w_0 \tag{32}$$

w_0 is the max wellbore width.C_L is leak-off coefficient, can be obtained from Mini-frac. S_p is the spurt loss,t is the injection time, and q_i is the injection rate.

2. Calculate injected volume of slurry

$$V_i = q_i \times t_e \tag{33}$$

Calculate fluid efficiency

$$\eta_e = \frac{V_{\text{fe}}}{v_i} = \frac{h_f x_f \bar{w}_e}{V_i} \tag{34}$$

In the second stage, the Proppant schedule is determined:

1. Calculate the exponent of the proppant concentration curve

$$\varepsilon = \frac{1-\eta}{1+\eta} \tag{35}$$

where ε is proppant exponent.

2. Calculate the pad volume and the time needed to pump it

$$V_{pad} = \varepsilon V_i \tag{36}$$

$$t_{pad} = \varepsilon t_e \tag{37}$$

3. Calculate required final proppant concentration:

$$c_e = \frac{M}{\eta V_i} \tag{38}$$

4. The required proppant concentration (mass/unit injected slurry volume) is

$$c = c_e \left(\frac{t - t_{pad}}{t_e - t_{pad}} \right)^{\varepsilon} \tag{39}$$

where c_e is the maximum proppant concentration.

5. Convert concentration into proppant added to frac fluid

$$c_{added} = \frac{c}{1 - \frac{c}{\rho_p}} \tag{40}$$

6. Fracturing fluid rate

$$q_i\left(1-\frac{c_{added}}{\rho_p}\right) \tag{41}$$

7. Checks

   7.1. Sum of pumped proppant should be *M*, mass of proppant

   7.2. Sum of volume of proppant and volume of clean liquid should be V_i

$$w_p = \frac{M}{\left(1-\phi_p\right)\rho_p x_f h_f} \tag{42}$$

3. METHODOLOGY

According to the equilibrium height concept, fracture toughness at the tip equals the rock intensity factor calculated from Eq. (27) and Eq. (28). The *p*-3D model of Pitakbunkate (2010) found out the equilibrium by solving Eq. (27) and Eq.(28) , which as mentioned earlier has some drawbacks. One issue illustrated in Figure 2 is that the final equilibrium solution can lie out of the valid range of original equilibrium height, in which case, artificial constraints are set to ensure model stability.

To avoid instability, this study starts with discretizing all the containment layers, then examining all possible fracture heights within the accuracy of the discretization. 2D model is used to calculate the net pressure. Then this net pressure is used as an input in the LEFM module to verify if it matches input height.

Figure 13 is the dimensionless schematic of an n-layer reservoir, where m layers are cracked.

For those layers locating above half fracture height, $\frac{h_f}{2}$, let d_k be the depth of k^{th} layer, then the dimensionless vertical position of layer *k*, b_k , is:

$$b_k = \begin{cases} 1 - \frac{d_k - d_s}{\frac{hf}{2}} & , d_k - d_s <= \frac{hf}{2} \\ -1 + \frac{d_e - d_k}{\frac{hf}{2}} & , d_k - d_s > \frac{hf}{2} \end{cases} \quad (43)$$

where *s*, *e* represent the layer number of top , bottom bounding layer, the number of cracked number, *m*, equals *e* - *s*.

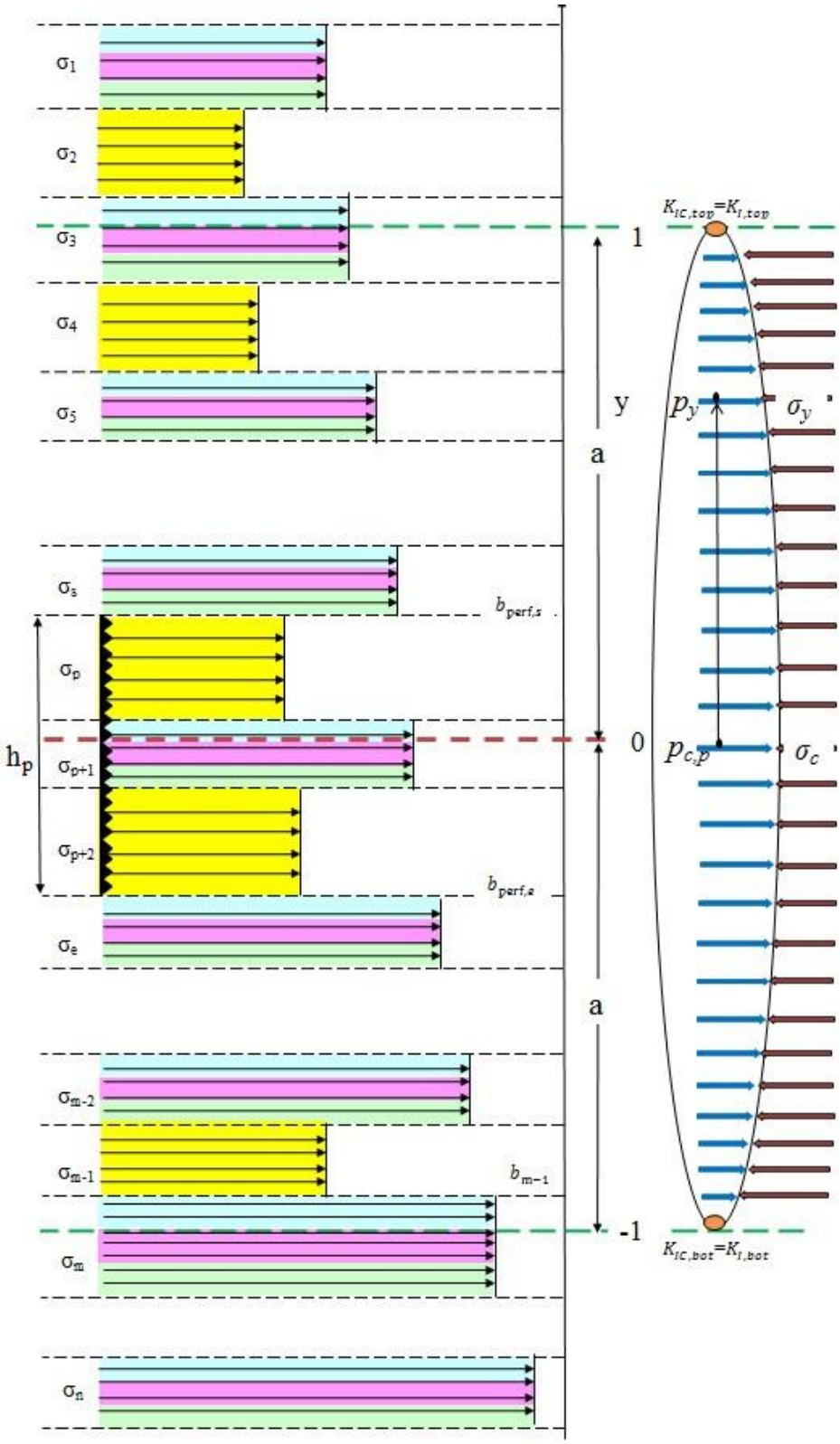

Figure 13:Fracture height growth in an n-layer reservoir and it stops at the stress equilibrium

Note, aside from the ideal case in which the fracture center is located at the perforation center, a fracture may grow upwards or downwards at a different extent, due to the variation of rock properties and the hydrostatic pressure inside the fracture. That may lead to a separation of the center of the perforations from the vertical center of the created fracture.

The factor to convert dimensionless to non-dimensionless system is

$$\frac{1}{a} = \frac{b_{\text{perf},s} - b_{\text{perf},e}}{h_p} \tag{44}$$

where $b_{\text{perf},s}$ and $b_{\text{perf},e}$ are dimensionless locations of the start and end of perforation layer, respectively.

Substitute Eq.(44) into Eq. (27) to get the intensity factor calculation from the dimensionless system:

$$K_I = \sqrt{\frac{h_p}{\pi(b_{\text{perf},s} - b_{\text{perf},e})}} \times \int_{-1}^{1} p_n(y) \sqrt{\frac{1+y}{1-y}}\, dy \tag{45}$$

$p_n(y)$ in Eq.(45) represents the net pressure at any dimensionless vertical position, *y*. It can be described as the difference of treating pressure at the center of the crack, $p_{c,y}$, and minimum in-situ stress at *y* location, as Figure 13. The treating pressure at the center of perforation crack, $p_{c,p}$, is the summation of pressure at the center of crack at *y* location and hydrostatic pressure.

$$p_{n,y} = p_{c,y} - \sigma_y \tag{46}$$

$$p_{c,p} = p_{c,y} + \rho g y \tag{47}$$

Combining Eq. (46) and Eq.(47) , the net pressure at *y* location is

$$p_{n,y} = p_{c,p} - \rho g y - \sigma_y \tag{48}$$

where $p_{c,p}$represents pressure at the center of perforated layer, $p_{c,y}$ is pressure at the crack center of location *y*.

At the perforated layer, according to Eq. (46)

$$p_{c,p} = p_{n,c} + \sigma_c \tag{49}$$

Plugging Eq. (49) into Eq.(48) and using the dimensionless factor, Eq. (48) becomes:

$$p_{n,y} = p_{n,c} + (\sigma_c - \sigma_y) + k_1 y_d \tag{50}$$

where k_1 is the hydrostatic gradient:

$$k_1 = -\rho g \frac{h_p}{b_{perf,s} - b_{perf,e}} \tag{51}$$

and $p_{c,p} = p_{n,c} + \sigma_c$ is the treating pressure.

The term $(\sigma_c - \sigma_y)$ in Eq. (50) clearly shows the importance of layers stress contrast to the crack behavior.

According to the Equilibrium Height concept, Eq.(28), the fracture will be contained in the upper and lower layer if Eq.(52) and Eq.(53) can be solved simultaneously:

$$K_{I,top} = K_I = \sqrt{\frac{h_p}{\pi(b_{perf,s} - b_{perf,e})}} \times \int_{-1}^{1} p_n(y) \sqrt{\frac{1+y}{1-y}} dy \tag{52}$$

$$K_{I,bot} = K_I = \sqrt{\frac{h_p}{\pi(b_{perf,s} - b_{perf,e})}} \times \int_{-1}^{1} p_n(y) \sqrt{\frac{1-y}{1+y}} dy \tag{53}$$

Only the dimensionless position pair $(b_{\text{perf},s}, b_{\text{perf},e})$ meets the pressure equilibrium, i.e. it satisfies two constraints Eq.(52) and Eq. (53). Consequently, the dimensional penetrations into the upper (Δh_u) and lower (Δh_d) layers can be calculated. The fracture height can be computed using Eq.(54)

$$h_f = h_p + \Delta h_u + \Delta h_d \tag{54}$$

To deliver optimum fracture geometry, fracture height, width and half-length, this study suggests the following height calculation procedure.

The basic idea is as the procedure given in Eq. (55). For each possible fracture height, h_{input} in Figure 14, use UFD model and fracture propagation model to calculate the required net pressure. This net pressure will uniquely yield a crack with height of h_{output} in Figure 14, according to LEFM. The net pressure bridges h_{input} and h_{output} ,and the height convergence is pursued in the design procedure.

$$h_{\text{input}} \underset{\rightarrow}{1} p_{\text{net}} \underset{\rightarrow}{2} h_{\text{output}} \tag{55}$$

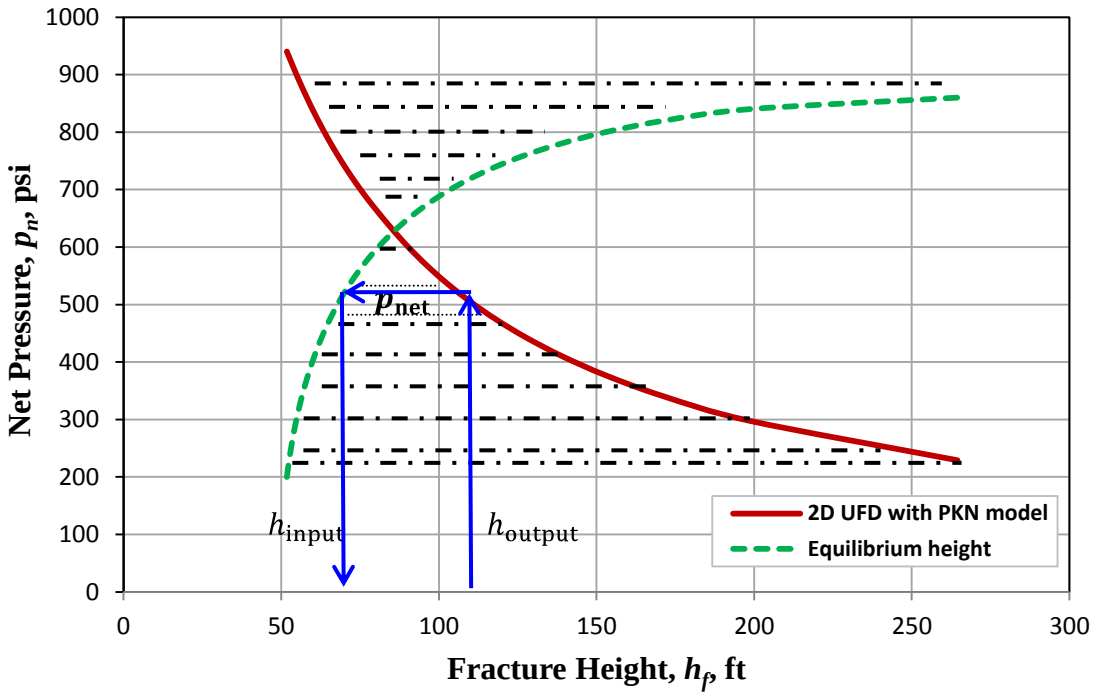

Figure 14:**Incorporating rigorous height determination into the 2D UFD (Pitakbunkate et al., 2011)**

This study uses an iterative process with a number of height combinations to complete the procedure 2 of Eq. (55), based on the following explanation.

Recall, the equilibrium height concept is to solve Eq.(28) at the top and bottom fracture tip, in other words, to minimize K_{error} in Eq. (56) .

$$K_{error} = |(K_I - K_{IC})_{top}| + |(K_I - K_{IC})_{bottom}| \quad (56)$$

where K_I is defined in Eq. (45) and its components change as the top and bottom tip change, i.e, the equation errors of Eq. (56) have jumps in such cases. The discontinue nature of the equation error makes it difficult to use traditional equation solving algorithms. Instead of solving the two equations, this study divides each containment layer into several ones, and plugs them into the Eq. (56) to pick up the layer pair with smallest equation error.

The discrete number should be chosen properly to compromise between precision and computational workload. In the attached example, the containment layer are thin, 20 ft at most, therefore, one-to-three layers division are used. The number should be adjusted according to the thickness in the real case.

However, in high rate gas well, when non-Darcy effect is involved, due to iteration calculation of the effective permeability, the number of iterative calculations of a smaller layer-discretization will be increased dramatically.

The following is the detailed procedure, as flow chart (Figure 15) illustrates:

1. Layer data processing.
    1.1. Containment layer discretization. All the possible containment layers will be discretized and paired in the way that each pair consists of a top and a bottom bounding layer.
    1.2. Dimensionless location calculation for each layer, Eq. (43) .

1.3. Other calculated results. Net height (Note: net height changes depending on the number of pay layers), in-situ stress, permeability, fracture toughness, plain stress.

2. h_f to p_{net}

For each pair, use the 2D model to calculate fracture half-length and width. Then calculate the net pressure from the hydraulic width (Step 1 in Eq. (55)).

2.1. Unified Fracture Design (UFD). Calculate the proppant number (N_p), optimum dimensionless fracture conductivity ($C_{fD,opt}$) and maximum dimensionless productivity index ($J_{D,max}$), fracture half length ($x_{f,opt}$) and fracture width ($w_{f,opt}$), Eq. (16) through Eq. (26) describe the optimization procedure.

2.2. Fracture half-length and width calculation.

2.2.1. PKN-type fracture geometry. Eq. (4) through Eq. (12)

2.2.2. KGD-type fracture geometry. Eq. (13) through Eq. (15)

2.3. Calculate net pressure. Eq. (4)

3. p_{net} to h_f

Use the calculated net pressure from step 3) as an input to LEFM. Calculate the fracture height, (Step 2 in Eq. (55)).

3.1. For each containment pair, plug in the dimensionless location calculated from Step 1.2 with Eq. (43) into Eq.(52) and Eq.(53). Get the stress intensity factors at the top, $K_{I,Top}$, and bottom layer, $K_{I,Bot}$.

3.2. Compare the calculated stress intensity factors, $K_{I,Top}$ and $K_{I,Top}$ from Step 3.1) with the fracture toughness, $K_{Ic,Top}$ and $K_{Ic,Bot}$, for each containment pairs. Generate a K_{error} set, Eq. (56).

3.3. Choose containment pair with Min(K_{error})

4. Equilibrium height.

Compare the fracture height input to Step 2) and fracture height output from Step 3), the height convergence is the solution, the shaded area in Figure 14 is H_{error} of Eq. (57)

$$H_{error} = Abs(H_{input} - H_{output}) \tag{57}$$

5. Output

5.1. Plug the calculated height from Step 4) into UFD model, to get the optimum planar geometry, productivity index, fracture conductivity, aspect ratio, using Eq. (16) through Eq. (22)

5.2. Generate pumping schedule with Eq. (31) through Eq. (42)

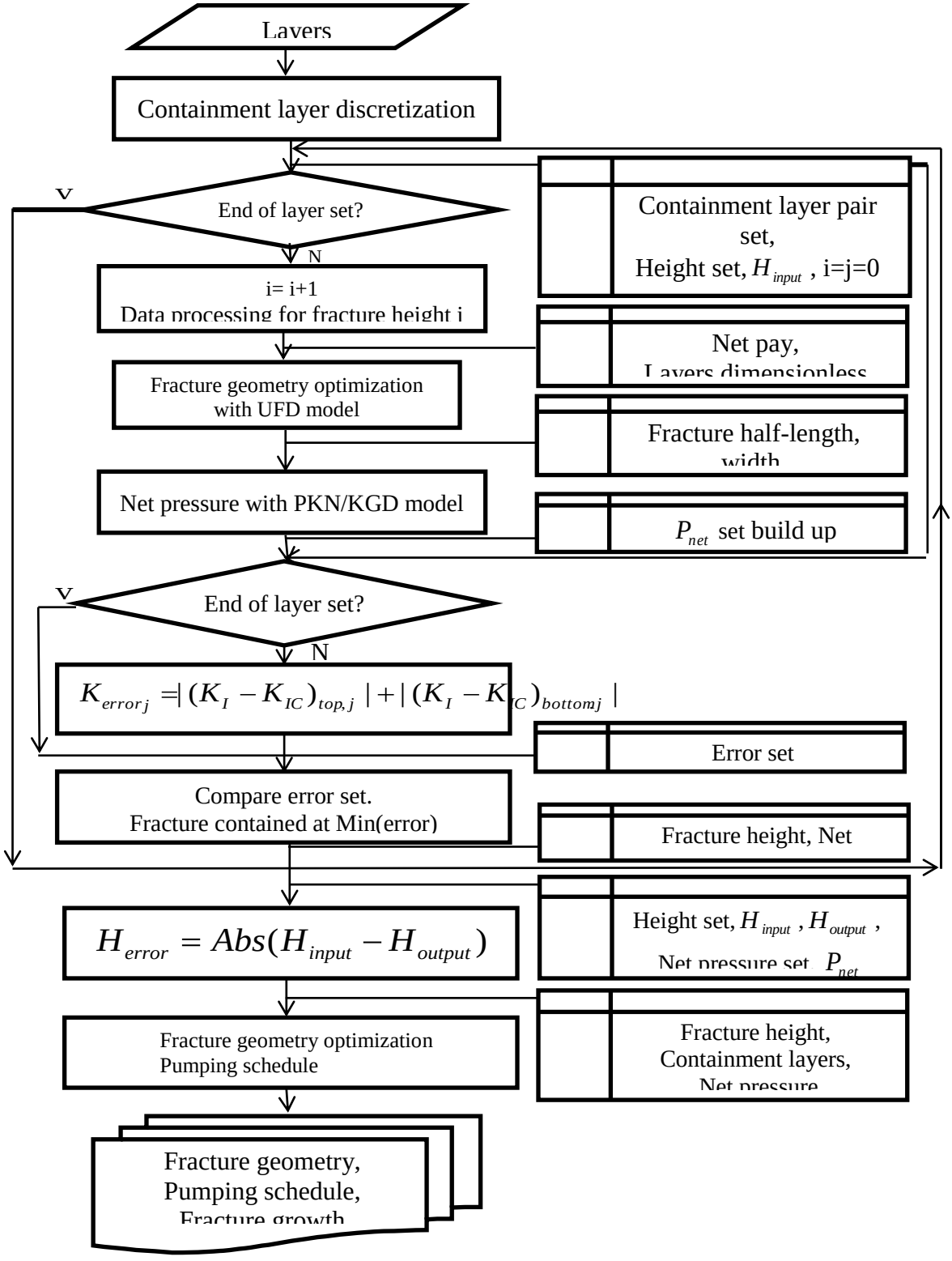

Figure 15:Multilayer *p*-3D Fracture design and optimization flow chart

The followings are three sample calculations of the proposed model, two for oil and one for a gas reservoirs respectively. The job size is fixed for all designs, as Table 1. Fracture gradient is 0.9 psi/ft and 0.6 psi/ft for containment layer and pay layer respectively.

Table 1 : Reservoir and fracture job input data for the fracture designs

Well radius, r_w, ft	0.375
Proppant mass, M_p, lbm	200,000
Porosity of proppant pack	0.36
Specific gravity of proppant	3.56
Proppant pack permeability, k_f, md	287,000
Proppant damage factor	0.5
K_{pr} , $lbf.s^{npr}\ ft^2$	0.4
n_{pr}	0.26
Injection rate, bpm	30

3.1. Sample Calculation I —Oil Well

The following fracture design is for a shallow (4,000 ft TVD) conventional oil reservoir with vertical well. The pay zone permeability is 1 md, drainage area 80 acres. Other reservoir parameters are listed in Table 1. Table 2 is the layer information; the original 15-layer reservoir is discretization into a 30-layers one, each possible containment layer being divided into three candidate layers. Possible fracture height equilibrium may happen at any combination of the top and bottom layer, i.e. The top containment layer can be any layer from layer number 1 to number 7 in this example and the bottom one can be from layer number 13 to number 30.

The design results are shown in Table 3, Table 4, Figure 17 and Figure 18.

Table 2 : Layer information after discretization for sample I, oil well

Layer	Depth ft	Thickness ft	Lithology	σ psi	ν	K_{IC} psi $\sqrt{inch}$	Perforation	E' psi	k md
1	4000	7	Shale	3600	0.3	1000	0	1E+06	0.001
2	4007	7	Shale	3606	0.3	1000	0	1E+06	0.001
3	4013	7	Shale	3612	0.3	1000	0	1E+06	0.001
4	4020	20	Sand	2412	0.25	1200	0	5E+06	1
5	4040	2	Shale	3636	0.3	1000	0	1E+06	0.001
6	4042	1	Shale	3638	0.3	1000	0	1E+06	0.001
7	4043	2	Shale	3639	0.3	1000	0	1E+06	0.001
8	4045	20	Sand	2427	0.25	1200	1	5E+06	1
9	4065	2	Shale	3659	0.3	1000	1	1E+06	0.001
10	4067	2	Shale	3660	0.3	1000	1	1E+06	0.001
11	4068	2	Shale	3662	0.3	1000	1	1E+06	0.001
12	4070	50	Sand	2442	0.25	1200	1	5E+06	1
13	4120	2	Shale	3708	0.3	1000	0	1E+06	0.001
14	4122	1	Shale	3710	0.3	1000	0	1E+06	0.001
15	4123	2	Shale	3711	0.3	1000	0	1E+06	0.001
16	4125	20	Sand	2475	0.25	1200	0	5E+06	1
17	4145	2	Shale	3731	0.3	1000	0	1E+06	0.001
18	4147	1	Shale	3732	0.3	1000	0	1E+06	0.001
19	4148	2	Shale	3734	0.3	1000	0	1E+06	0.001
20	4150	20	Sand	2490	0.25	1200	0	5E+06	1
21	4170	2	Shale	3753	0.3	1000	0	1E+06	0.001
22	4172	1	Shale	3755	0.3	1000	0	1E+06	0.001
23	4173	2	Shale	3756	0.3	1000	0	1E+06	0.001
24	4175	20	Sand	2505	0.25	1200	0	5E+06	1
25	4195	2	Shale	3776	0.3	1000	0	1E+06	0.001
26	4197	1	Shale	3777	0.3	1000	0	1E+06	0.001
27	4198	2	Shale	3779	0.3	1000	0	1E+06	0.001
28	4200	15	Sand	2520	0.25	1200	0	5E+06	1
29	4215	2	Shale	3794	0.3	1000	0	1E+06	0.001
30	4217	1	Shale	3795	0.3	1000	0	1E+06	0.001
31	4218	2	Shale	3797	0.3	1000	0	1E+06	0.001

Table 3 : Fracture design results for sample I, oil well

Proppant number, N_p	1.45	Fracture height, h_f, ft	110
Dimensionless productivity index, $J_{D,opt}$	0.96	Fracture half-length, x_f, ft	644
Fracture penetration ratio, $I_{x,opt}$	0.69	Fracture width, w_f, inch	0.16
Dimensionless conductivity, $c_{fd,opt}$	3.03	Pad time, t_{pad}, min	32
Fracture aspect ratio	11.39	Pumping time, t_e, min	57
Slurry efficiency, η_e	0.28	Net pressure, p_n, psi	1,120
Nolte, ϵ	0.56	$c_{add,end}$,ppga	14

Table 4 : Pumping schedule for sample I, oil well

□	Start minute	End minute	C_{add} ppga	C_e ppg	Mass of proppant lbm	Liquid volume gal
Pad	0	45	0	0	0	56,234
1	45	46	1	1	2,202	2,202
2	46	48	2	2	3,395	1,698
3	48	51	3	3	10,369	3,456
4	51	53	4	4	9,192	2,298
5	53	57	5	4	19,370	3,874
6	57	59	6	5	14,902	2,484
7	59	63	7	6	27,695	3,956
8	63	65	8	6	19,777	2,472
9	65	69	9	7	34,889	3,877
10	69	72	10	7	23,631	2,363
11	72	75	11	8	34,578	3,143

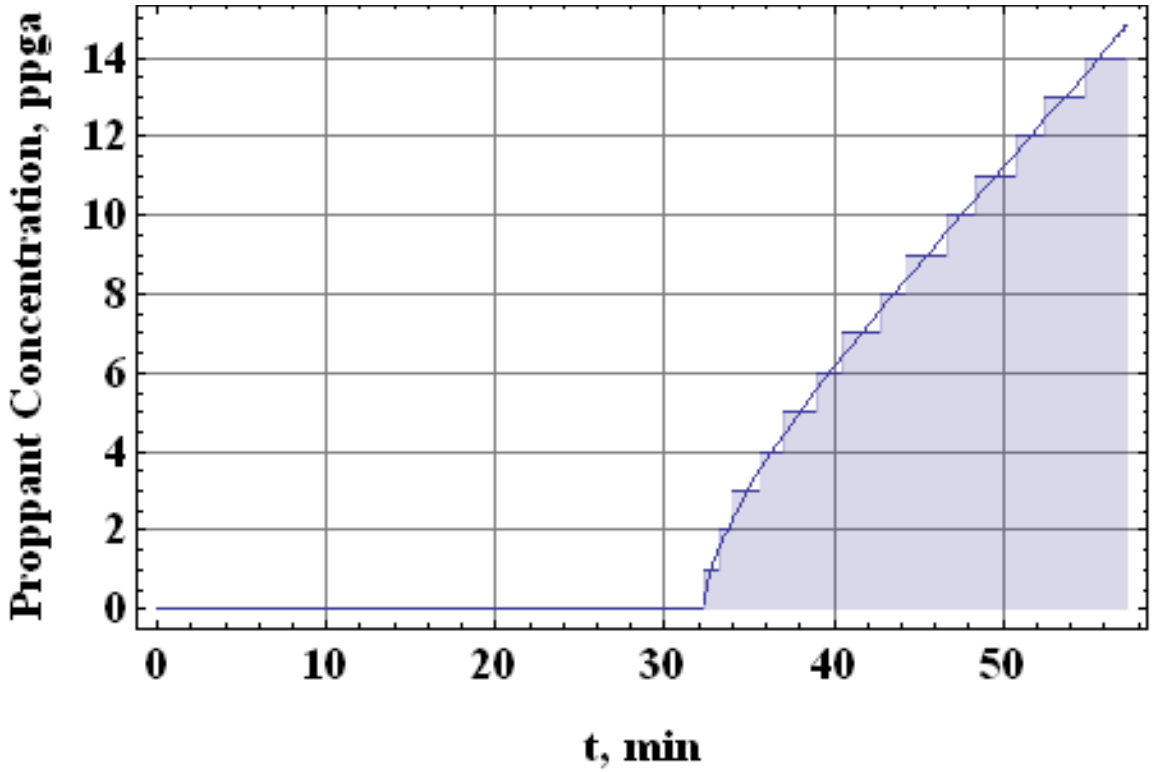

Figure 16:Discretized proppant added concentration schedule for oil well I

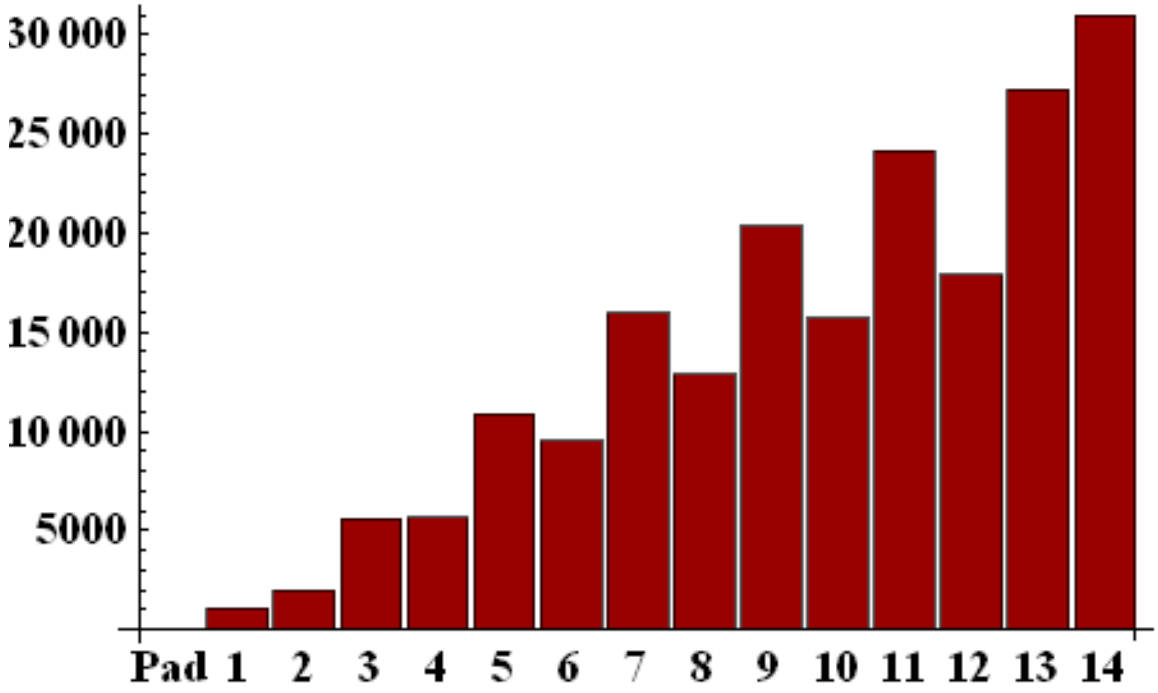

Figure 17:Proppant mass at each stage in lb for sample I, oil well

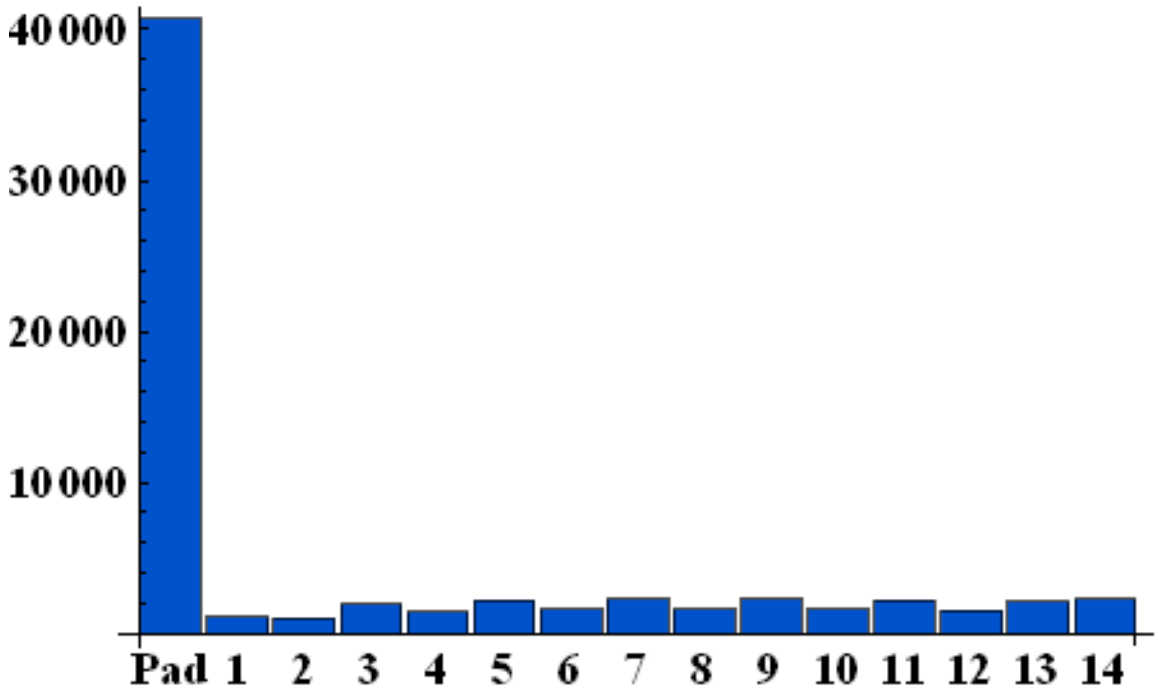

Figure 18:Clean liquid volume at each stage in gal for sample I, oil well

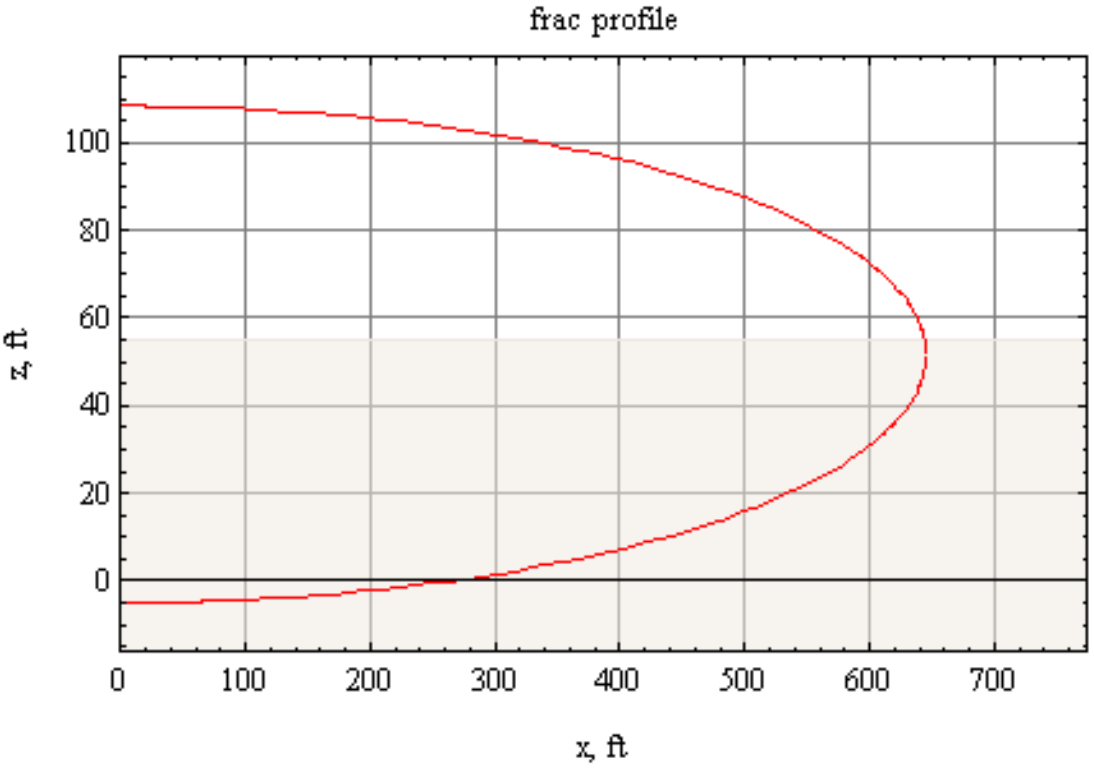

Figure 19:Fracture placement for sample I, oil well

3.2. Sample Calculation II —Gas Well

The following fracture design is for a 8,000 ft TVD gas reservoir with vertical well. The pay zone permeability is 1 md and the drainage area 160 acres. Other reservoir parameters are listed in Table 1.

As discussed in Section 2, non-Darcy effects are considered in this design and the effective permeability is calculated.

Table 5 is the layer information; the original 7-layer reservoir is discretized into 14-layers, each possible containment layer being divided into three candidate layers. Possible fracture height equilibrium may happen at any combination of the top and bottom layer, i.e., the top containment layer can be any layer from layer number 1 to number 3 in this example and the bottom one can be from layer number 9 to number 14.

The design results are in

Table 6, Table 7, Figure 21 and Figure 23. The resulting proppant pack effective permeability is 20,000 md, compared with the permeability of 144,000 md, which is a result of applying 0.5 damage factor to the original nominal permeability of 287,000 md.

Table 5 : Layer information after discretization for sample II, gas well

Layer	Depth ft	Thickness ft	Lithology	σ, psi	ν	K_{IC} psi $\sqrt{\text{inch}}$	Perforation	E' psi	k md
1	8000	23	Shale	7,200	0.3	1000	0	1E+06	0.001
2	8023	23	Shale	7,221	0.3	1000	0	1E+06	0.001
3	8047	23	Shale	7,242	0.3	1000	0	1E+06	0.001
4	8070	50	Sand	4,842	0.25	1200	1	5E+06	1
5	8120	2	Shale	7,308	0.3	1000	1	1E+06	0.001
6	8122	2	Shale	7,310	0.3	1000	1	1E+06	0.001
7	8123	2	Shale	7,311	0.3	1000	1	1E+06	0.001
8	8125	45	Sand	4,875	0.25	1200	1	5E+06	1
9	8170	2	Shale	7,353	0.3	1000	0	1E+06	0.001
10	8172	2	Shale	7,355	0.3	1000	0	1E+06	0.001
11	8173	2	Shale	7,356	0.3	1000	0	1E+06	0.001
12	8175	20	Sand	4,905	0.25	1200	0	5E+06	1
13	8195	8	Shale	7,376	0.3	1000	0	1E+06	0.001
14	8203	8	Shale	7,383	0.3	1000	0	1E+06	0.001
15	8212	8	Shale	7,391	0.3	1000	0	1E+06	0.001

Table 6 : Fracture design results for sample II, gas well

Effective permeability, md	20,000	Fracture height, h_f, ft	153
Proppant number, N_p	0.084	Fracture half-length, x_f, ft	482
Dimensionless productivity index, $J_{D,opt}$	0.45	Fracture width, w_f, inch	0.3
Fracture penetration ratio, $I_{x,opt}$	0.22	Pad time, t_{pad}, min	26
Dimensionless conductivity, $c_{fd,opt}$	1.64	Pumping time, t_e, min	50
Fracture aspect ratio	6	Net pressure, p_n, psi	800
Slurry efficiency, η_e	0.32	$c_{add,end}$, ppga	15
Nolte, ϵ	0.52		

Table 7 : Pumping schedule for sample II, gas well

□	Start minute	End minute	C_{add} ppga	C_e ppg	Mass of proppant lbm	Liquid volume gal
Pad	0	26	0	0	0	32,494
1	26	26	1	1	713	713
2	26	27	2	2	1,708	854
3	27	28	3	3	4,355	1,452
4	28	30	4	4	5,303	1,326
5	30	31	5	4	9,076	1,815
6	31	33	6	5	9,345	1,558
7	33	35	7	6	13,848	1,978
8	35	36	8	6	13,185	1,648
9	36	38	9	7	18,223	2,025
10	38	40	10	7	16,551	1,655
11	40	42	11	8	22,028	2,003
12	42	44	12	9	19,358	1,613
13	44	46	13	9	25,230	1,941
14	46	48	14	10	21,610	1,544
15	48	50	15	10	19,467	1,298

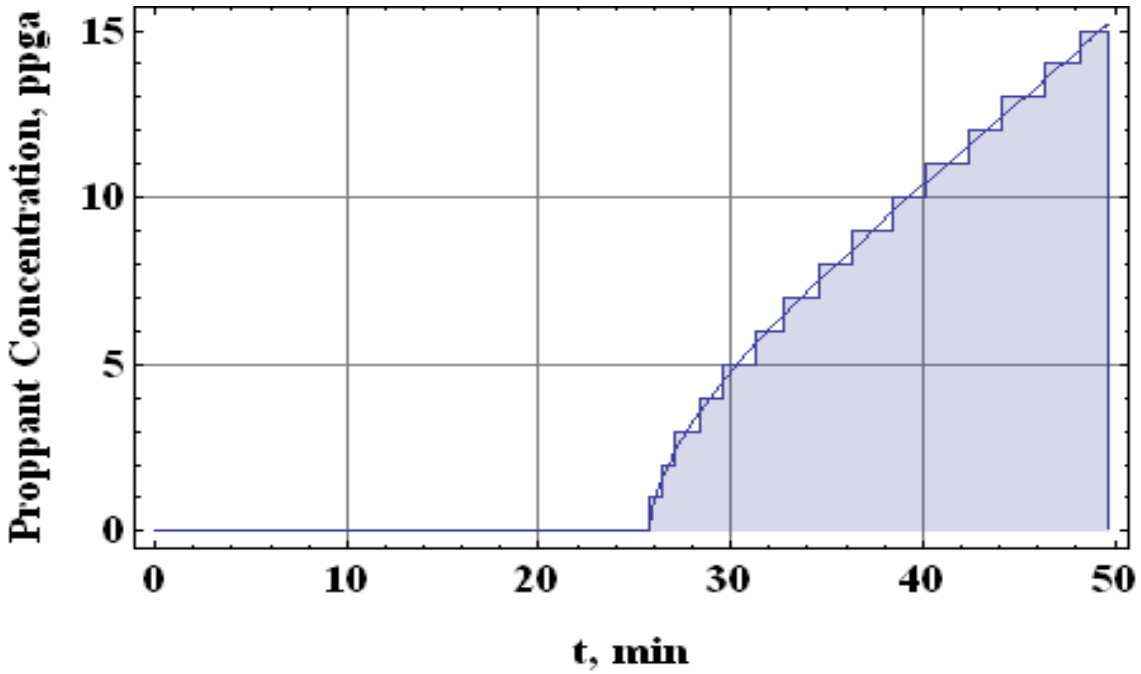

Figure 20:Discretized proppant added concentration schedule for sample II, gas well

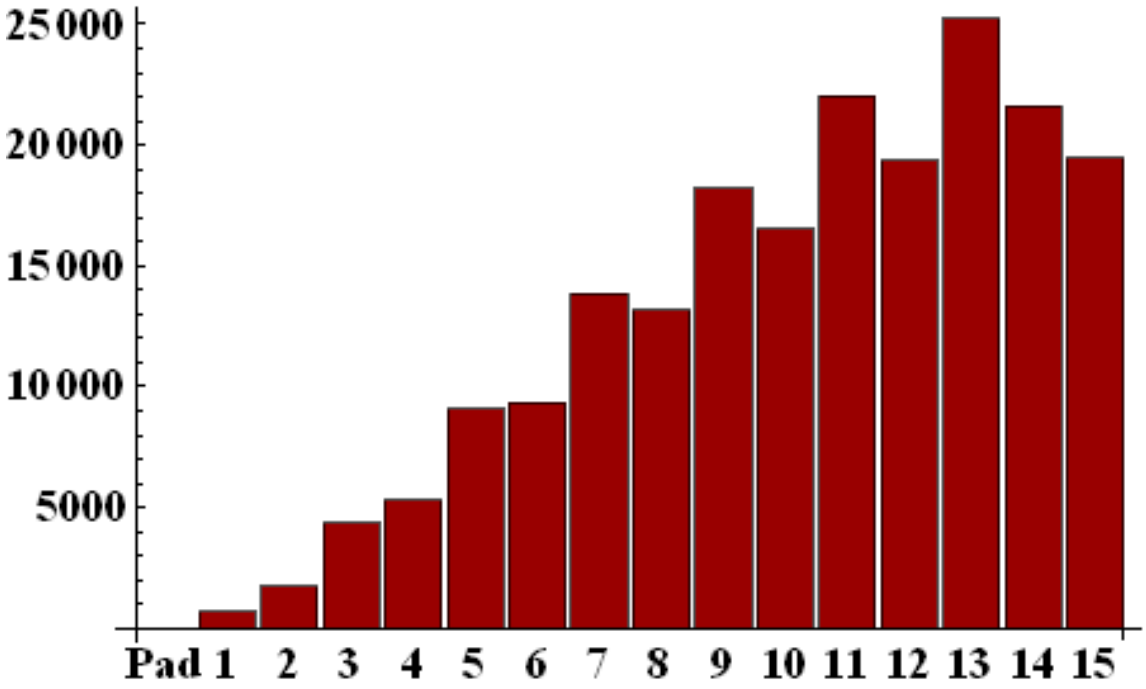

Figure 21:Proppant mass at each stage in lb for gas well

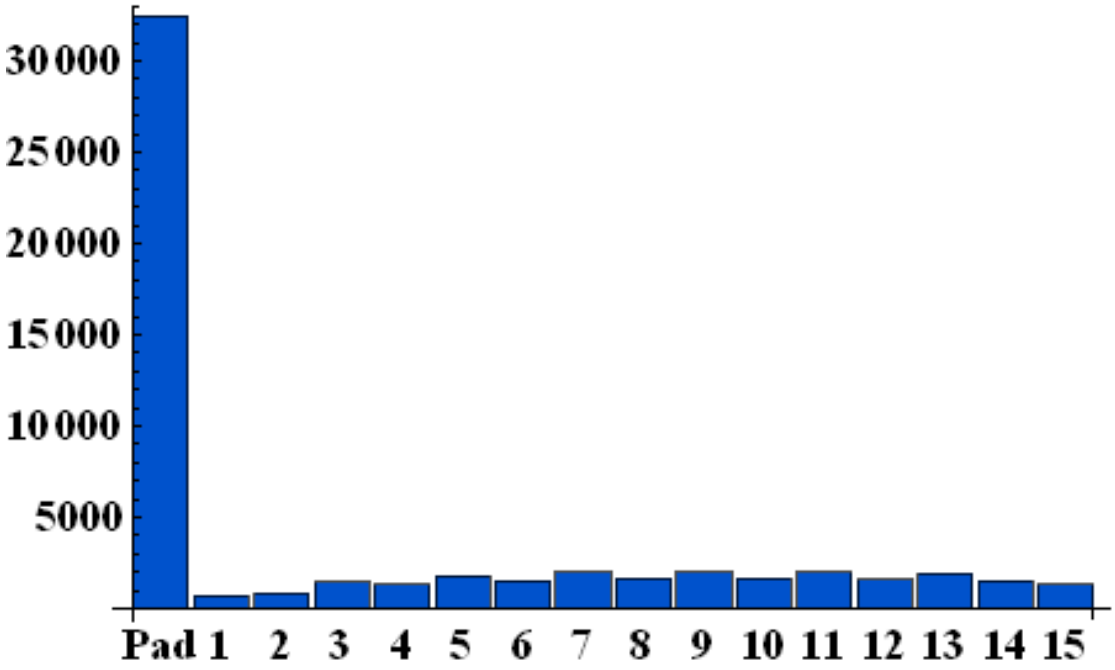

Figure 22:Clean liquid volume at each stage in gal for sample II, gas well

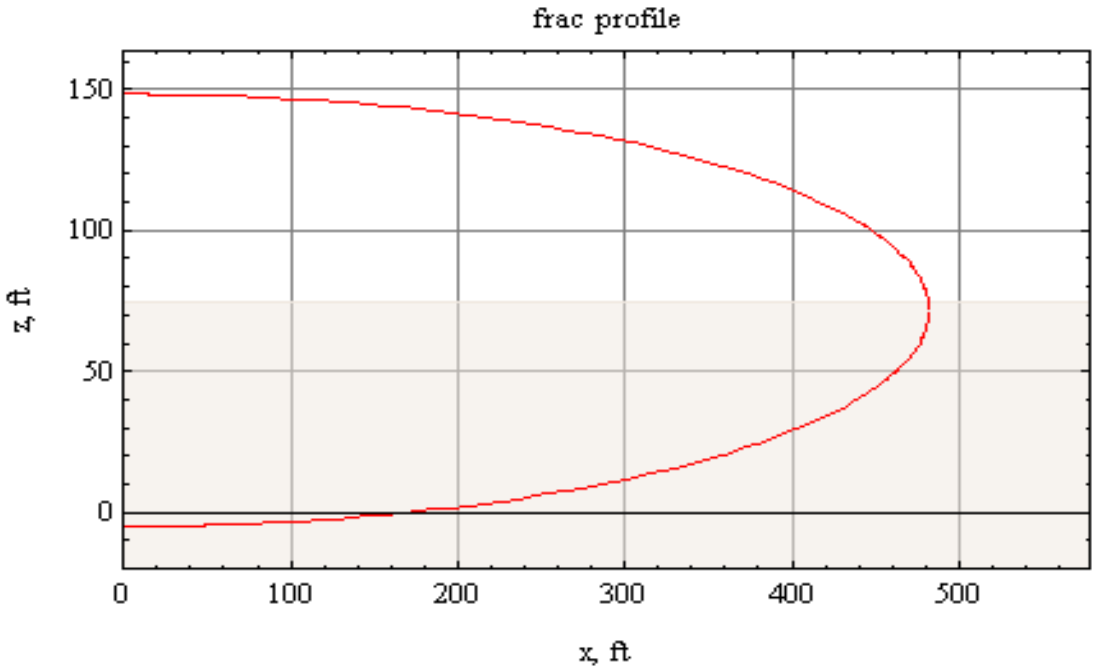

Figure 23:Fracture placement, gas reservoir for sample II, gas well

3.3. Sample Calculation III—Oil Well

The third fracture design is for an oil vertical well with aquifer underneath.

The pay zone permeability is 50 md, drainage area 80 acres. Note the rock property is different from the above cases; the Young's modulus in this example is 2×10^6 psi instead of 5×10^6 psi. Other reservoir and fracture job parameters are listed in Table 1.

Table 8 is original layer information, the perforated interval is in green and the aquifer is in blue, 35 meters away from the bottom of perforation. Figure 24 through Figure 26 are the log map.

The design results are in Table 10 and Table 11 and Figure 27 through Figure 29.

Table 8 : Original reservoir information for sample III, oil well

No	Depth,		thick.	Gamma ray	Neutral density	Bulk density	High resistivit	Low resistivit	poros ϕ	satur. S_w	perm. k	Fluid type
	m		m	Api	%	g/cc	Ωm	Ωm	%	%	md	
1	3600	3633.1	33.1	60.3	15.1	2.50	4.3	3.5	7.9	100.0	3.1	Dry
2	3633.	3635.8	2.7	67.2	18.3	2.40	6.8	8.4	14.9	65.3	28.9	oil
3	3635.	3660.6	1.6	60.3	15.1	2.50	4.3	3.5	7.9	100.0	3.1	Dry
4	3660.	3663.8	3.2	62.3	19.4	2.33	10.8	12.4	18.7	61.6	134.9	oil
5	3663.	3674.9	11.1	60.3	15.1	2.50	4.3	3.5	7.9	100.0	3.1	Dry
6	3674.	3678.5	3.6	62.1	21.6	2.27	5.9	5.5	22.3	69.2	290.5	oil
7	3678.	3680.2	1.7	60.3	15.1	2.50	4.3	3.5	7.9	100.0	3.1	Dry
8	3680.	3681.0	0.8	59.6	17.9	2.33	7.7	7.5	18.0	66.1	114.6	oil
9	3681.	3685.1	1.0	57.2	14.4	2.44	14.3	18.4	9.2	87.0	16.7	Dry
10	3685.	3687.0	1.9	69.1	16.6	2.38	14.2	13.0	12.9	61.9	26.8	Oil
11	3687.	3694.8	7.8	60.3	15.1	2.50	4.3	3.5	7.9	100.0	3.1	Dry
12	3694.	3700.0	1.4	60.3	14.9	2.45	6.5	5.8	11.1	77.1	15.3	Oil
13	3700.	3703.3	3.3	77.7	16.6	2.50	3.9	3.8	5.1	100.0	0.5	Dry
14	3703.	3709.3	6.0	62.9	19.1	2.31	10.2	9.5	18.7	51.1	144.2	Oil
15	3709.	3727.9	18.9	77.7	16.6	2.50	3.9	3.8	5.1	100.0	0.5	Dry
16	3727.	3729.6	1.7	53.8	12.3	2.46	11.4	11.1	11.5	74.2	16.4	Oil
17	3729.	3734.7	1.8	77.9	13.5	2.44	3.7	3.6	9.5	100.0	8.6	Dry
18	3734.	3737.8	3.1	62.2	15.0	2.39	5.9	5.4	14.6	63.2	45.1	oil
19	3737.	3742.9	1.5	69.7	18.2	2.47	3.4	3.2	7.8	100.0	5.4	Dry
20	3742.	3745.1	2.2	64.3	15.0	2.41	6.2	5.5	12.9	62.8	30.4	oil
21	3745.	3753.7	4.7	56.7	19.0	2.35	3.0	2.5	17.8	95.9	111.6	Water & oil

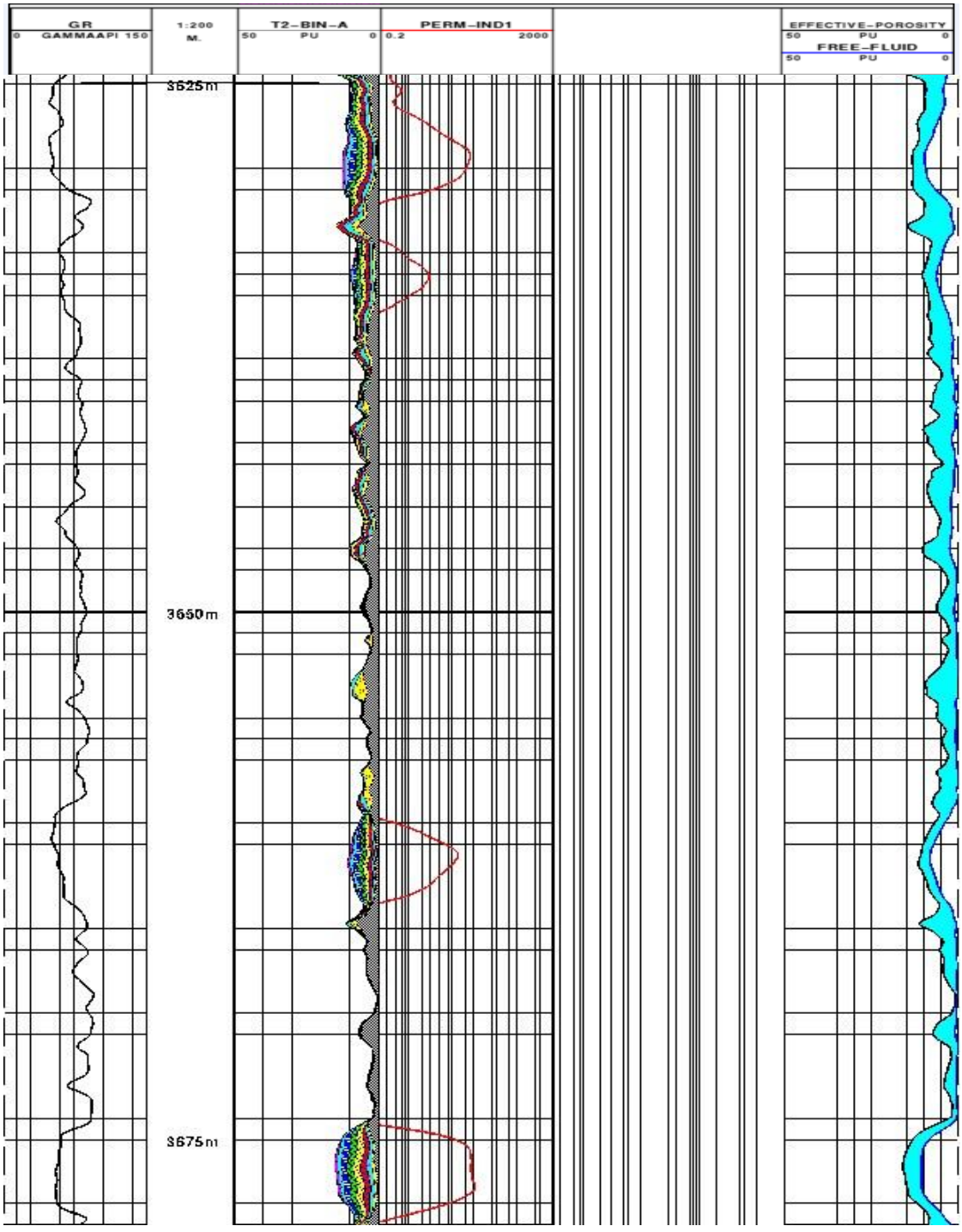

Figure 24:**Log track (3625 m~ 3675 m)**

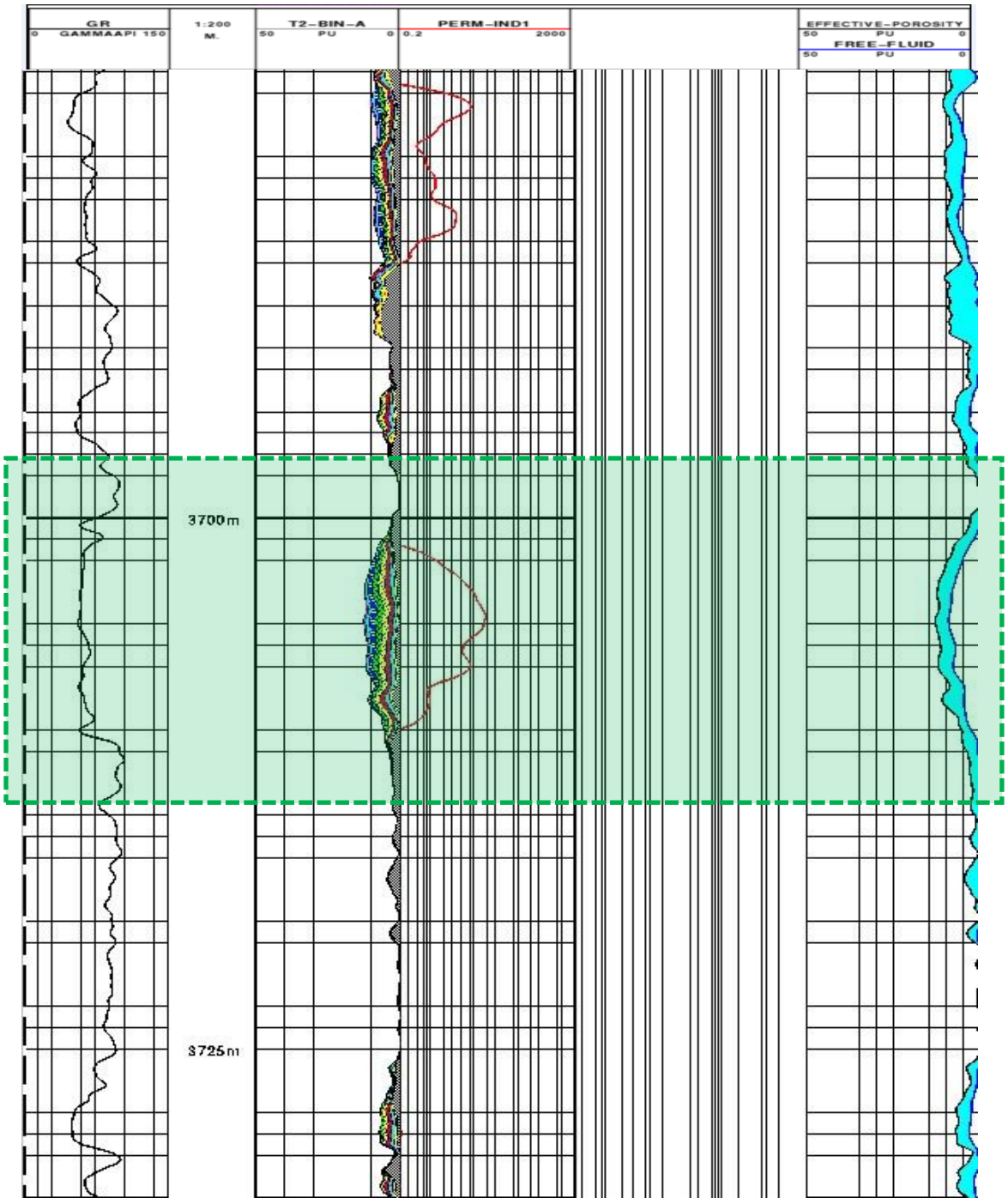

Figure 25:Log track (3675 m~ 3725 m)

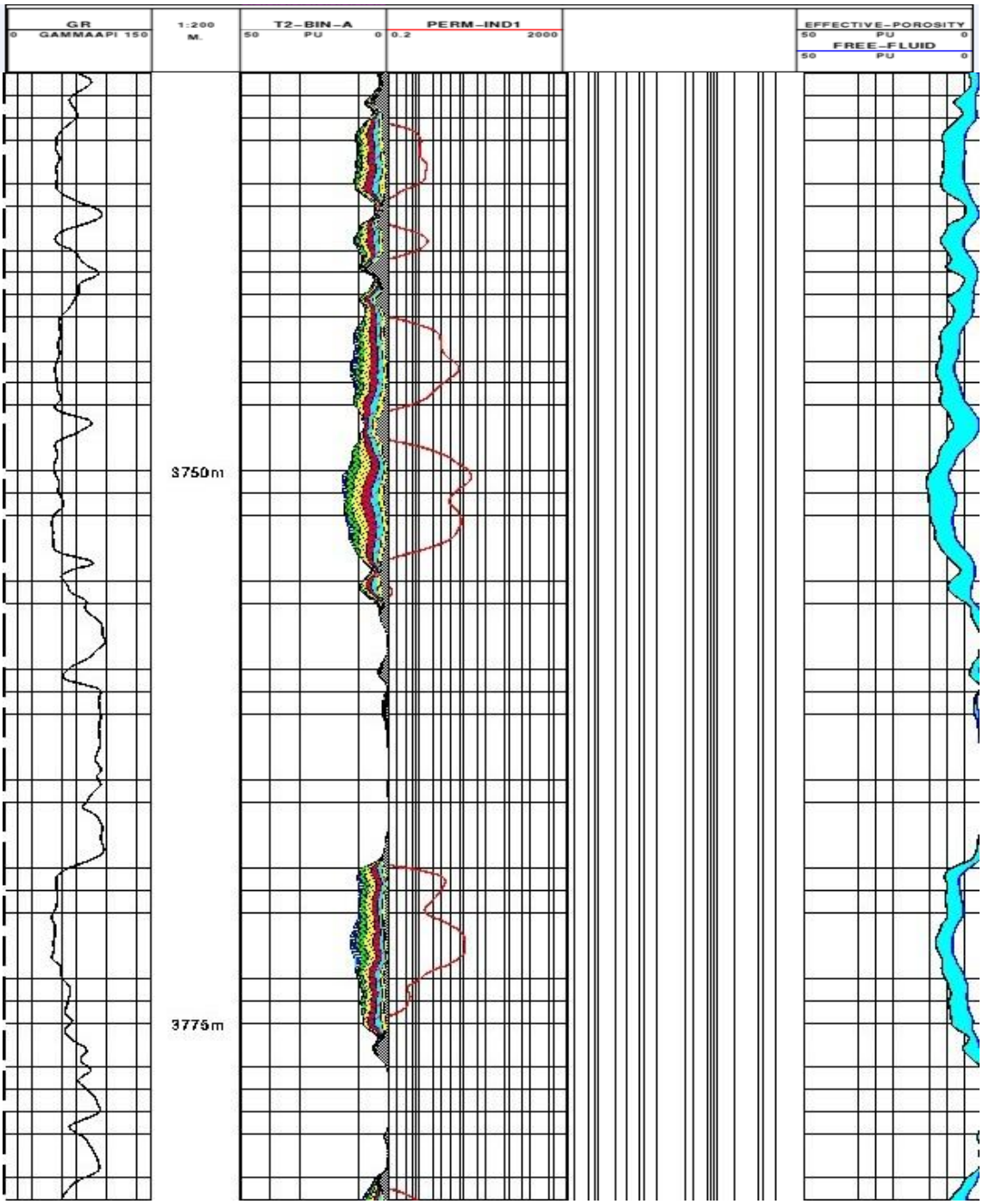

Figure 26:Log track (3725 m~ 3780 m)

3.3.1 Design Results

Table 9 : Layer information after discretization for sample III, oil well

Layer	Depth m	Thickness m	Lithology	σ, psi	ν	K_{IC} psi $\sqrt{inch}$	Perforation	E' psi	k md
1	3600	11	Shale	10,630	0.3	1000	0	1E+06	0.001
2	3611	11	Shale	10,663	0.3	1000	0	1E+06	0.001
3	3622	11	Shale	10,695	0.3	1000	0	1E+06	0.001
4	3633	3	Sand	7,152	0.26	1200	0	2E+06	50
5	3636	8	Shale	10,736	0.3	1000	0	1E+06	0.001
6	3644	8	Shale	10,760	0.3	1000	0	1E+06	0.001
7	3652	8	Shale	10,784	0.3	1000	0	1E+06	0.001
8	3661	3	Sand	7,206	0.26	1200	0	2E+06	50
9	3664	4	Shale	10,818	0.3	1000	0	1E+06	0.001
10	3668	4	Shale	10,829	0.3	1000	0	1E+06	0.001
11	3671	4	Shale	10,840	0.3	1000	0	1E+06	0.001
12	3675	4	Sand	7,234	0.26	1200	0	2E+06	50
13	3679	1	Shale	10,862	0.3	1000	0	1E+06	0.001
14	3679	1	Shale	10,863	0.3	1000	0	1E+06	0.001
15	3680	1	Shale	10,865	0.3	1000	0	1E+06	0.001
16	3680	1	Sand	7,244	0.26	1200	0	2E+06	50
17	3681	1	Shale	10,869	0.3	1000	0	1E+06	0.001
18	3682	1	Shale	10,873	0.3	1000	0	1E+06	0.001
19	3684	1	Shale	10,877	0.3	1000	0	1E+06	0.001
20	3685	2	Sand	7,254	0.26	1200	0	2E+06	50
21	3687	3	Shale	10,887	0.3	1000	0	1E+06	0.001
22	3690	3	Shale	10,894	0.3	1000	0	1E+06	0.001
23	3692	3	Shale	10,902	0.3	1000	0	1E+06	0.001
24	3695	5	Sand	7,273	0.26	1200	1	2E+06	50
25	3700	1	Shale	10,925	0.3	1000	1	1E+06	0.001
26	3701	1	Shale	10,928	0.3	1000	1	1E+06	0.001
27	3702	1	Shale	10,932	0.3	1000	1	1E+06	0.001
28	3703	6	Sand	7,290	0.26	1200	1	2E+06	50
29	3709	6	Shale	10,953	0.3	1000	0	1E+06	0.001
30	3716	6	Shale	10,971	0.3	1000	0	1E+06	0.001
31	3722	6	Shale	10,989	0.3	1000	0	1E+06	0.001
32	3728	2	Sand	7,338	0.26	1200	0	2E+06	50
33	3730	2	Shale	11,013	0.3	1000	0	1E+06	0.001
34	3731	2	Shale	11,018	0.3	1000	0	1E+06	0.001
35	3733	2	Shale	11,023	0.3	1000	0	1E+06	0.001
36	3735	3	Sand	7,352	0.26	1200	0	2E+06	50
37	3738	2	Shale	11,037	0.3	1000	0	1E+06	0.001
38	3740	2	Shale	11,042	0.3	1000	0	1E+06	0.001
39	3741	2	Shale	11,047	0.3	1000	0	1E+06	0.001

Table 9 Continued

40	3743	2	Sand	7,368	0.26	1200	0	2E+06	50
41	3745	3	Shale	11,058	0.3	1000	0	1E+06	0.001
42	3748	3	Shale	11,067	0.3	1000	0	1E+06	0.001
43	3751	3	Shale	11,075	0.3	1000	0	1E+06	0.001

Table 10:Fracture design results for sample III, oil well

Proppant number, N_p	0.028	Fracture height, h_f, m	33
Dimensionless productivity index, $J_{D,opt}$	0.36	Upwards migration, h_u, m	2.7
Fracture penetration ratio, $I_{x,opt}$	0.13	Downwards migration, h_d, m	12.5
Dimensionless conductivity, $c_{fd,opt}$	1.64	Fracture half-length, x_f, m	171
fracture aspect ratio($2x_f/h_f$)	10	Fracture width, w_f, cm	0.75
slurry efficiency, η_e	0.33	Pad time, t_{pad}, min	26
Nolte, ϵ	0.5	Pumping time, t_e, min	52
$c_{add,end}$, ppga	15	Net pressure, p_n, psi	326

Table 11:Pumping schedule for sample III, oil well

□	Start minute	End minute	C_{add} ppga	C_e ppg	Mass of proppant Lbm	Liquid volume gal
Pad	0	26	0	0	0	32,494
1	26	26	1	1	713	713
2	26	27	2	2	1,708	854
3	27	28	3	3	4,355	1,452
4	28	30	4	4	5,303	1,326
5	30	31	5	4	9,076	1,815
6	31	33	6	5	9,345	1,558
7	33	35	7	6	13,848	1,978
8	35	36	8	6	13,185	1,648
9	36	38	9	7	18,223	2,025
10	38	40	10	7	16,551	1,655
11	40	42	11	8	22,028	2,003
12	42	44	12	9	19,358	1,613
13	44	46	13	9	25,230	1,941
14	46	48	14	10	21,610	1,544
15	48	50	15	10	19,467	1,298

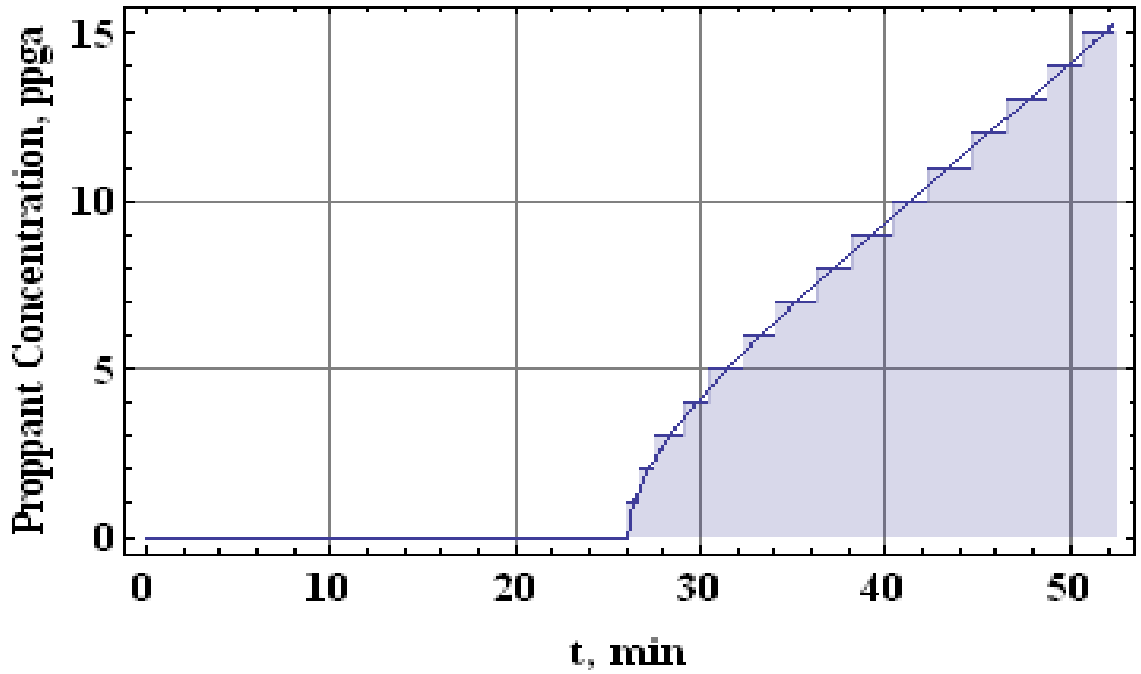

Figure 27 : Discretized proppant added concentration schedule for sample III, oil well

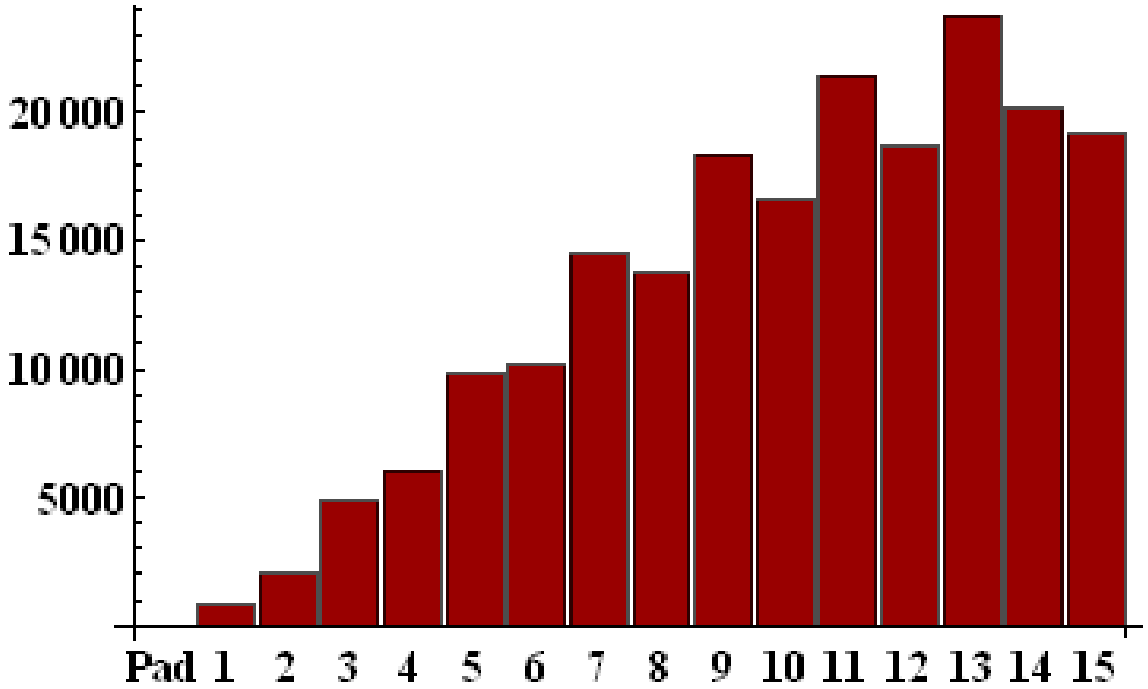

Figure 28 : Proppant mass at each stage in lb for sample III, oil well

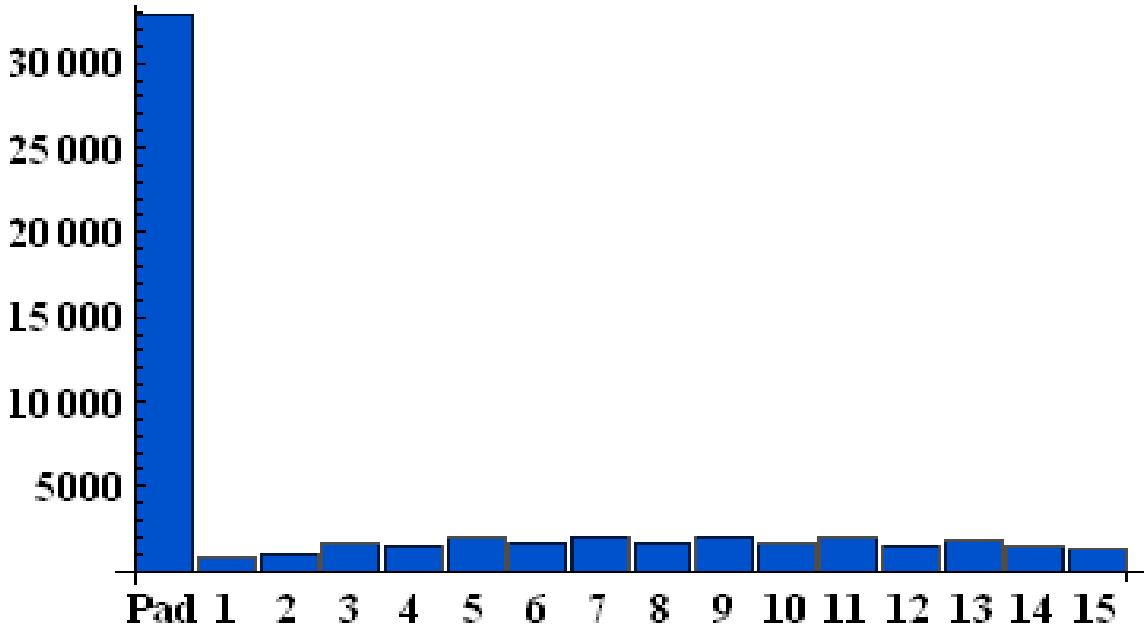

Figure 29:Clean liquid volume at each stage in gal for sample III, oil well

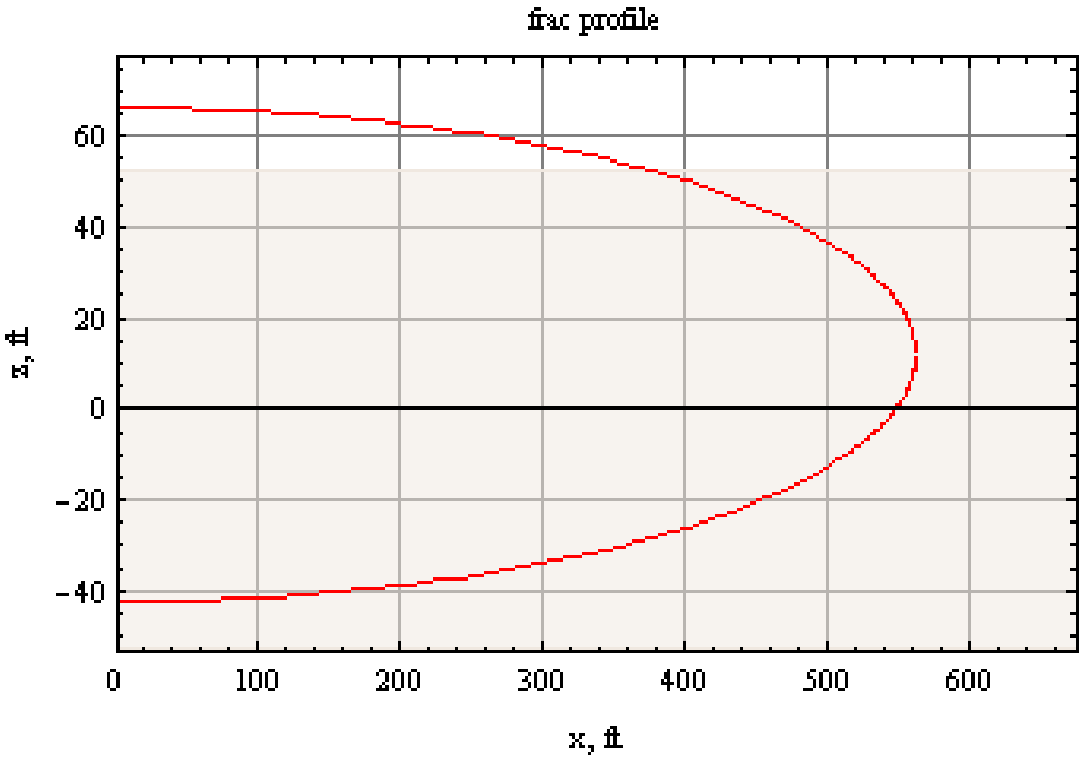

Figure 30:Fracture placement for sample III, oil well

3.3.2. Interpretation of Results

According to the last fracture design, if a net pressure of 326 psi is applied at the center of the reservoir, the fracture will not crack to the bottom aquifer. In other words, an amount of proppant and a given design should not exceed this net pressure, which will correspond to the optimized fracture geometry that would maximize the dimensionless productivity index.

The net pressure constraint to prevent fracture growth into the water bearing layer may be too limiting, preventing the draining of overlain layers containing oil. A second fracture stage should then be considered to generate another fracture above the perforated interval. For example, layers number 6 and 8 in Table 8, have high permeability and low water saturation and are good fracture candidates for a second perforated interval and a second fracture stage.

4. APPLICATION AND DISCUSSION

4.1. Application

The multi-layered *p*-3D fracture design is an integrated package. For a given fracture job size it can deliver a 3D optimized fracture geometry to maximize the productivity index.

Other by-products of this work include:

1. Elimination of arbitrary fracture height selection. The fracture height calculation part can be taken as a guide for other 2D fracturing design models by pointing out reasonable fracture containment layers of the reservoir.
2. Avoiding fracture height growth in unwanted layers. This is meaningful in maintaining zonal isolation after fracturing. For example, breaking into gas cap and/or aquifer can generate serious problems in oil well production. The fracturing job size should be chosen properly so that fracturing will not induce unintended zonal communication, i.e, avoiding fracture growth into the gas cap and water layers. This issue is important, no matter whether there is an ideal three layer reservoir or one consisting of fifteen layers. Figure 31 and Figure 32 illustrate net pressure and fracture heights according to the optimum fracture geometry from the fracture design based on different job size.

If there is a gas zone 30 ft above the perforated interval, the maximum allowed net pressure to avoid fracture propagation into the gas zone is approximately 550 psi (see Figure 31). Therefore, the fracture design that gives the final net pressure (where the solid

lines and the green dash line intersect) greater than 550 psi is not suitable. In this case, the design for 1,000,000 lbm of proppant mass gives the fracture invading the gas zone. Decreasing the size of treatment to 500,000 lbm or 200,000 lbm may help from producing gas from that zone.

Another illustration is if there is a water zone 30 ft below the target formation, the maximum allowed net pressure to avoid fracture propagation into the water zone is approximately 510 psi (see Figure 32). In this case, the design for 200,000 lbm of proppant mass is the only suitable option.

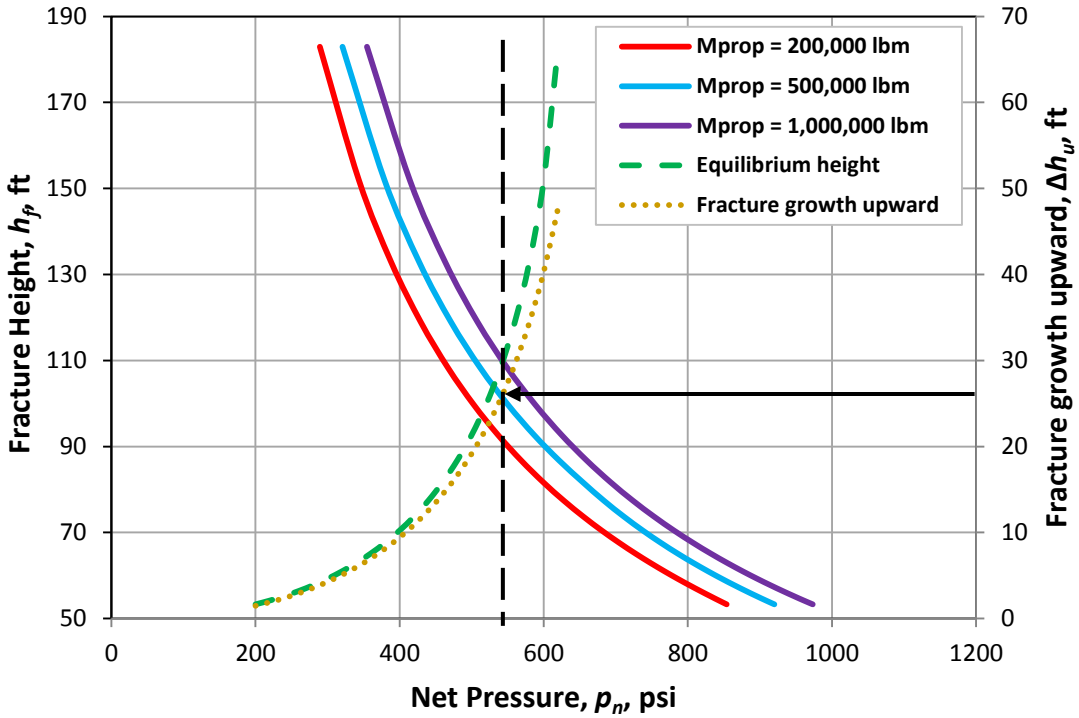

Figure 31:Example of application of *p*-3D to avoid fracture invading to gas zone (Pitakbunkate et al., 2011)

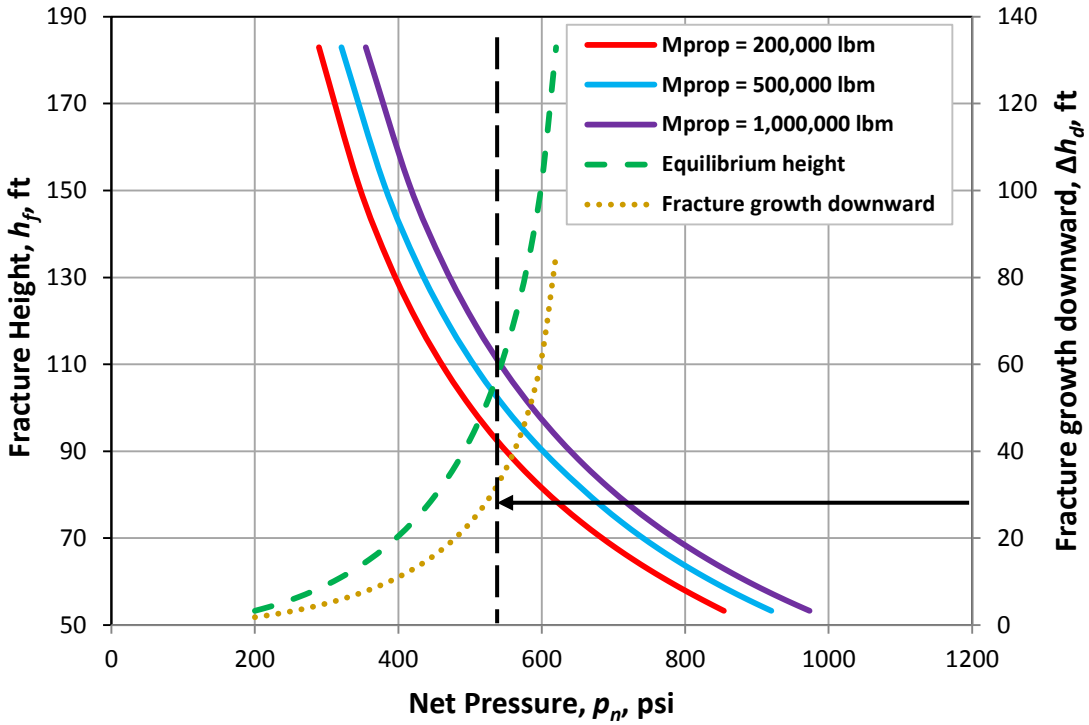

Figure 32:Example of application of p-3D to avoid fracture invading to aquifer (Pitakbunkate et al. 2011)

The sample Calculation III demonstrates how to use the multilayer *p*-3D to avoid aquifer.

4.2. Discussion

In-situ stress contrast between layers and individual layer fracture toughness are the keys to vertical fracture propagation. To obtain reservoir rock properties, for example, the Young's Modulus, a sonic log or a triaxial test in the laboratory should be done. Rock lithology analogy can be useful in assigning values to layers.

Mini-frac analysis can be used to calculate initial stresses; minimum in-situ stress, σ_h and maximum in-situ stress, σ_H, and leak-off coefficient. This research assumes that the difference between horizontal maximum and minimum in-situ stresses is sufficiently big that the fracture initiation will not have many choices.

The final fracture geometry should be verified with the help of seismic technology or, for fracture height, temperature logs which are not very reliable.

5. CONCLUSIONS

This study developed a methodology for multilayer *p*-3D fracture design. The proposed model integrated four parts, including containment layers discretization to get the possible fracture height candidates, Unified Fracture Design (UFD) model to calculate the fracture half-length and width, PKN/KGD model to calculate net pressure, and Linear Elastic Fracture Mechanics (LEFM) to calculate fracture height. The target is to find convergence of fracture height as well as that of net pressure.

This study begins with multiple containing layers discretization, to give potential fracture height.

With an assumed fracture height, and using UFD, to optimize the fracture half-length and width to achieve maximum productivity index the PKN or KGD models are employed to estimate a net pressure at the center of the perforation interval.

With the calculated net pressure, the layer properties, especially in-situ stress, using LEFM, a fracture height is calculated.

This height is compared to the originally assumed height. The procedure is repeated until there is a match.

Net pressure distribution serves as a bridge, linking the fracture height from 2D model and LEFM.

Other than maximizing production, another obvious application of this research is to prevent the fracture from propagating into the unintended layers (i.e. gas cap and aquifer).

Therefore, this study can guide fracture design job by pointing out:

(1) what treating pressure is needed to achieve the optimum fracture geometry;

(2) at which containment layers of the multi-layers will the vertical fracture propagation stop, given the above treating pressure;

(3) the layer discretization will allow an approximate location of the fracture top and bottom tips (i.e., 5 ft) which is sufficient for the purposes of this design.

REFERENCES

Cleary, M.P. 1994, Critical Issues in Hydraulic Fracturing of High-Permeability Reservoirs, paper SPE 27618 presented at the Aberdeen, United Kingdom,15-17 March, European Production Operations Conference and Exhibition

Economides, M.J., Oligney, R.E., and Valko, P.P. 2002. *Unified Fracture Design: Bridging the Gap between Theory and Practice*. Orsa Press, Alvin, TX

Economides, M.J., Oligney, R.E., and Valkó, P., 2002a "Applying Unified Fracture Design to Natural Gas wells." *World Oil*, pp 50-62

Economides, M.J. and Martin T., 2007, *Modern fracturing*, ET Publishing, Texas p.20-425

van Eekelen, H.A.M, 1982, Hydraulic Fracture Geometry: Fracture Containment in Layered Formations, *SPE Journal* 22: 341-349

Geetsma, J. and Haafkens, R. A, 1979, Comparision of the Theories for Predicting Width and Extent of Vertical Hydraulically Induced Fractures, *ASME*, 101 8-9

Griffith, A. A. 1921. *The phenomena of rupture and flow in solids.* Philosophical Transition, Series A, 221: 163-197.

Hubbert, M.K., and Willis, D.G. 1957. Mechanics of Hydraulic Fracturing. *Trans. AIME* 210: 153-166.

Irwin, G.R. 1957. Analysis of Stresses and Strains near the End of a Crack Traversing a Plate. *Journal of Applied Mechanics* 24: 361-364.

Johnson, D.E., Wright, and C.A., Cleary, M.P., 1993, On-Site Real-Time Analysis Allows Optimal Propped Fracture Stimulation of a Complex Gas Reservoir, *SPE* 25414

Khristianovitch, S. A., and Zheltov, Y. P., 1955, *Formation of Vertical Fractures by Means of Highly Viscous Fluids*, Proc.,World Pet. Cong., Rome (1955)2, 579–586,.

Lopez, H, P.P. Valko, and Pham, T., 2004, Optimum Fracture Treatment Design Minimizes the Impact of Non-Darcy Flow Effects, *SPE Annual Technical Conference and Exhibition*, SPE 90195

Orowan, E., 1952, Fundamentals of brittle behavior in metals, In *Fatigue and Fracture of Metals*, William M. Murray (ed.). 139-162, Wiley, New York

Perkins, T.K., and Kern, L.R. 1961. Width of Hydraulic Fractures. *JPT*, *Trans. AIME* 222: 937-949.

Pitakbunkate, T. 2010. Incorporating Rigorous Height Determination into Unified Fracture Design, M.S. thesis, Texas A&M University, College Station.

Pitakbunkate, T., Yang, M., Valkó, P.P. and Economides, M.J. 2011, Hydraulic Fracture Optimization with a p-3D model , SPE 142303

Rice, J.R. 1968. Fracture: An Advanced of Treatise. In Mathematical Analysis in the Mechanics of Fracture. H. Liewbowitz (ed.). 191-311, Academic Press, New York.

Simonson, E.R., Abou-Sayed, A.S. and Clifton, R.J. 1976. Containment of Massive Hydraulic Fractures. Paper SPE 6089-PA presented at the SPE Annual Technical Conference and Exhibition, New Orleans, 3-6 September. doi: 10.2118/6089-PA.

Smith, M.B., and Shlyapobersky, J.W. 2000. *Basic of Hydraulic Fracturing*. Reservoir Stimulation. Wiley, Malden, MA.

VITA

Name:	Mei Yang
Address:	Texas A&M University Petroleum Engineering Department 3116 TAMU 501 RICH College Station, Texas 77843-3116 Phone: 1-979-739-3812
Email Address:	mailtoym@gmail.com
Education:	B.Sc., Computer Science Guizhou University, 2001 Guiyang, P.R. China M.S., Math Computation Texas A&M University, 2009 M.S., Petroleum Engineering, Texas A&M University, 2011
Employment History:	Guizhou University, P.R China, 2001-2007

This thesis was typed by the author.